UNIVERSITÀ DEL PIEMONTE ORIENTALE

XXXII PhD Programme in Medical Sciences and Biotechnologies

(curriculum: Neoplastic, metabolic and age-related diseases)

Department of Health Science

PhD Thesis

# Targeted molecular characterization of adult midline and circumscribed gliomas for the identification of new potential targets for personalized therapy


Tutor

Professor Renzo Luciano Boldorini

Candidate

Dr Elena Trisolini


Academic year 2018 - 2019

# INDEX

# 1. INTRODUCTION

## 1.1 Diffuse midline glioma

Diffuse midline gliomas (MLGs) are infiltrative gliomas, mainly with an astrocytic differentiation, which affect midline structures of central nervous system (CNS): cerebellum, ventricles, thalamus, hypothalamus, pineal region, pons, spinal cord and brainstem[1]. MLGs occur more frequently in paediatric patients and young adults, while in adults fewer than 10% of diffuse gliomas arise in midline structures.

MLG typically harbour a missense mutation, p.Lys27Met, in H3 histone family member 3A (H3F3A) and histone cluster 1 H3 family member B (HIST1H3B) genes. H3F3A (1q42.12) and HIST1H3B (6p22.2) genes encode variants of the histone H3 protein, which is responsible for chromatin structure and consequently for gene expression. While HIST1H3B mutations are anatomically restricted to brainstem[2,3], H3F3A mutants have been reported in MLG of various locations[2,4-9], and other histone variants (e.g. H3F3A p.Gly34Val) occur in a subset of hemispheric supratentorial pediatric high-grade gliomas[2,3,8,10]. In pediatric MLGs, mutations in histone H3 variants associate with more aggressive clinical phenotype and poorer prognosis[6,8,11]. Based on these observations, histone H3-mutant gliomas progressively emerged as a phenotypically and molecularly separated group of tumours. The WHO 2016 classification subsequently introduced “diffuse midline glioma, H3K27M-mutant” as a new grade IV entity, even in the absence of histopathological markers of anaplasia (i.e. mitotic figures, microvascular proliferation and necrosis)[12].

Histone protein mutations contribute to gliomagenesis in this subgroup of tumours. Histone proteins are modified by the polycomb repressive complex 2 (PRC2) methyltransferase and by lysine (K)-specific demethylase (KDM). PRC2 increases methylation of Lys27, which promotes a more compact and transcriptionally repressed chromatin state. Whereas, KDM demethylase complex removes methyl groups from Lys27, promoting an open and transcriptionally active chromatin state. Histone H3K27M mutant protein binds PRC2 histone methyltransferase and functionally inactivates it, leading to a global reduction of Lys27 methylation, thereby promoting an open chromatin structure that favours a deregulated gene transcription[13] (Figure 1). Nowadays, an inhibitor (GSKJ4) of a protein composing KDM

demethylase complex is under study; this molecule is able to increases Lys27 methylation and so it suppresses gene expression and reduces tumour growth[14].

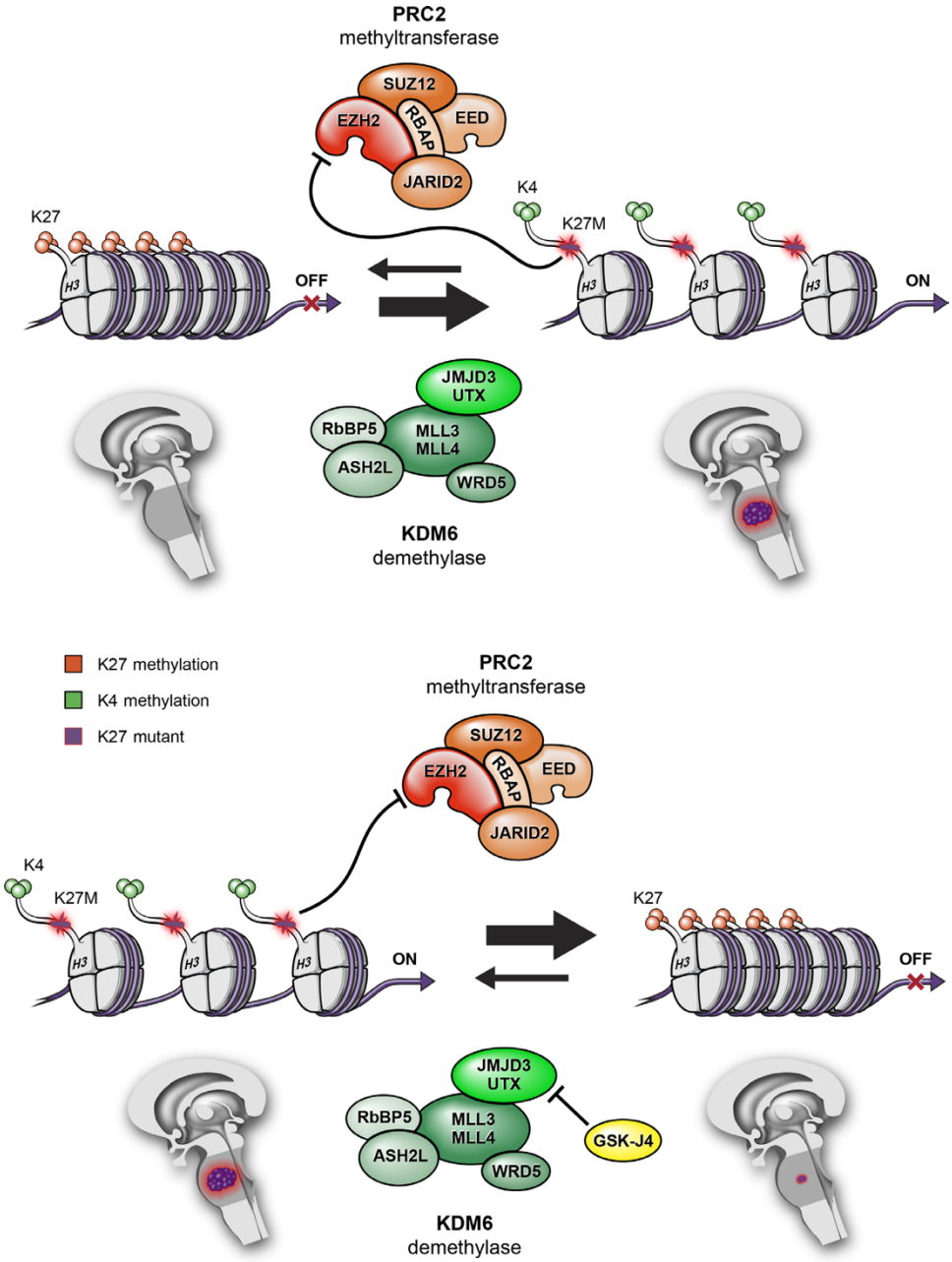


**Figure 1.** Histone modifications by PRC2 methyltransferase and KDM demethylase activities, and associations with transcriptionally active versus inactive states[13].

According to a 2016 WHO classification update[15], the term "diffuse midline glioma, H3 K27M-mutant" should be reserved for tumours that are diffuse (infiltrating), midline (thalamus, brain stem, spinal cord, etc.), gliomas and harbouring H3K27M mutation; it is important to remark that not each CNS tumour that harbours H3K27M mutation is a diffuse midline glioma. Histologically, MLG can resemble astrocytic (30% of all

MLGs), oligodendrocytic or other CNS tumours. In the past was known that H3K27M mutation was exclusively of MLG, nowadays, there are a number of tumours that are not diffuse midline gliomas which reported the same H3K27M mutation, including ependymomas, pilocytic astrocytomas, pediatric diffuse astrocytomas and gangliogliomas[15]. Authors showed that there is a group of gliomas that displays high-grade histology and clinical features and imaging of diffuse midline gliomas but do not harbours H3K27M mutation; it has been proposed to introduce H3K27M-wild-type tumour entity into WHO classification of CNS tumours[2].

In paediatric patients, MLGs have a more aggressive clinical phenotype and poorer prognosis, which is not associated with H3K27M mutation but probably with the age of onset. Indeed, studies confirm that there is no association between this mutation and a worst overall survival (OS) at any age. The poor prognosis is also due to the difficult access to tumour site for surgery[16].

While few studies specifically investigated the molecular landscape of adult MLG, recent works suggested that this subset of tumours may present with phenotypic and molecular characteristics differing from both pediatric MLG and adult supratentorial gliomas. As an illustration, although H3F3A mutations have been reported in adult MLG of the thalamus, hypothalamus, pineal region, brainstem, cerebellum and spinal cord[7,14,17-20], their prognostic significance in adults remains unclear[17,18]. Whole-exome sequencing analysis of 20 adult MLG identified recurrent mutations in TP53, H3F3A and ATRX while HIST1H3B and ACVR1 were not found[21]. Although less frequent, IDH1 and FGFR1 hotspot mutations represent particular interest in this population[21,22], because small molecule inhibitors targeting these mutants are being developed and there is an urgent need for new treatments in this disease[23,24].

Overall, the genomic landscape of adult MLG remains poorly understood, due to the rarity of the disease in this population and the lack of available histological material. Indeed, despite growing evidence indicating significant clinical and genomic heterogeneity among adult midline tumours[25], the need for histological confirmation in presence of a typical radiological presentation is often debated, because of the morbidity and mortality of surgical procedures in midline locations and assumption that histological diagnosis would only have limited impact on therapeutic management[20].

Other mutations in canonical cancer pathways frequently target the receptor tyrosine kinase RAS / PI3K pathway (e.g. mutations in PDGFRA, PIK3CA, PIK3R1, or PTEN; occurring in -50% of cases), the p53 pathway (e.g. mutations in TP53, PPM1D, CHEK2, or ATM; occurring in 70% of cases), and to a lesser extent the retinoblastoma protein pathway[26-28]. Activating mutations or fusions targeting FGFR1 were specifically identified in a small proportion of thalamic high-grade gliomas (10%)[29]. In contrast, recurrent mutations in ACVR1, the gene encoding the BMP receptor ACVR1, were detected in a subset (-20%) of diffuse intrinsic pontine gliomas (DIPGs), and seem to correlate with H3.1 mutations[26-28].

Concerning structural variations, high-level focal amplifications detected in diffuse midline gliomas include amplification of PDGFRA (in as many as 50% of DIPGs), MYC/MYCN (in as many as 35%), CDK4/6 or CCND1-3(in 20%), ID2 (in 10%), and MET (in 7%), whereas homozygous deletion of CDKN2A/B or loss of RB1 or NF1 is detected only very rarely (in < 5% of cases)[12]. Fusion events involving the tyrosine kinase receptor gene FGFR1 occur in thalamic diffuse gliomas, and a small proportion (4%) of paediatric pontine gliomas have been found to carry neurotrophin receptor (NTRK) fusion genes. Common broad chromosomal alterations include single copy gains of chromosome 1q and chromosome 2. In addition, there may be a subset of pontine gliomas (as many as 20%) that harbour few copy number changes[26,28,30].

### 1.1.1 Diagnosis

Main clinical signs and symptoms at diagnosis are progressive cognitive disorders and focal deficits, seizure (mainly in young patients), increase of intracranial pressure, cephalalgy, epilepsy and other behavioural disturbances[31].

The first examination is a computed tomorgaphy (CT) to confirm the presence of a lesion. After a positive result, the patient is submitted to magnetic resonance imaging (MRI) with contrast to highlight the lesion and its morphology. Then to evaluate the metabolic status of the lesion, positron emission tomography (PET) with F-fluorodeoxyglucose contrast is assessed. Moreover, in low grade gliomas the uptake slightly increases compared to normal tissue, whereas in high grade gliomas, the uptake increases significantly. According to these findings, PET results allow glioma grading[31,32].

For the characterization of the tumour, a needle biopsy is required for morphologic and molecular biology analyses. This procedure is usually reserved for patients with multiple co-morbidities whom could not tolerate a large cranial surgery or for those with unresectable tumours due to its location[33].

The algorithm below (Figure 2) shows the workflow assessed for an integrated diagnosis of glioma:

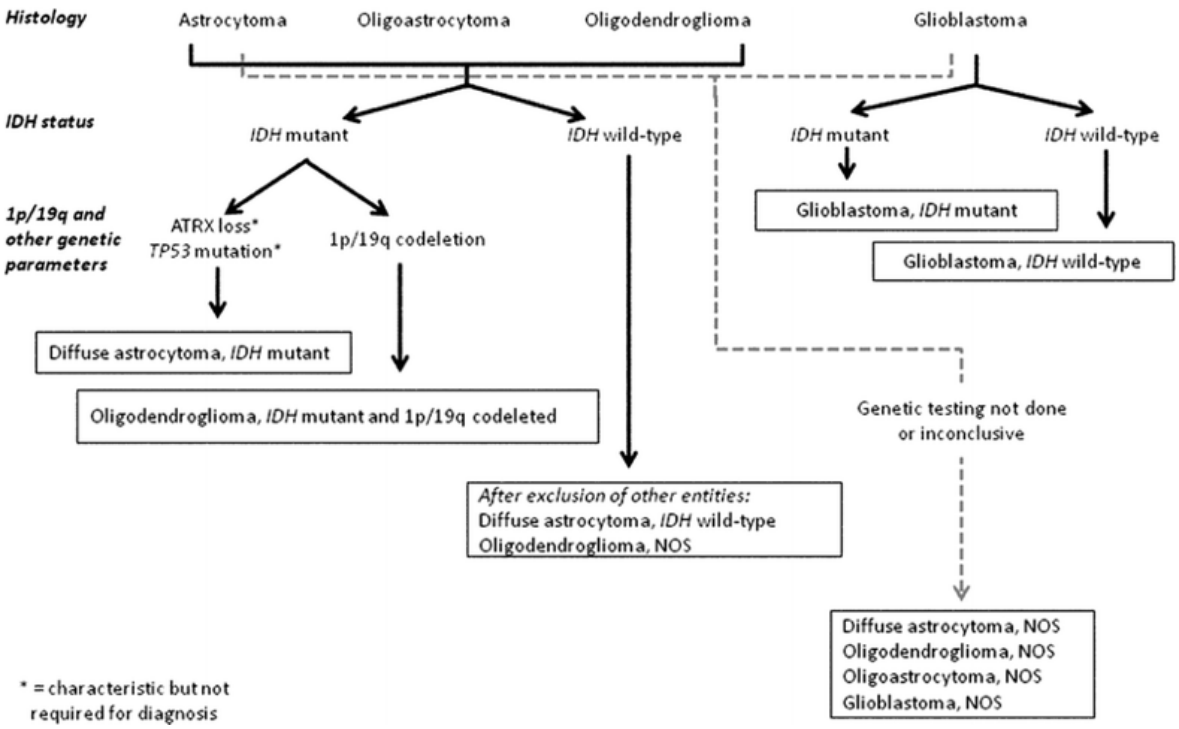


**Figure 2.** Algorithm to classify the diffuse gliomas based on histological and genetic features. Genetic profile characterization is fundamental to achieve an "integrated" diagnosis. A similar flow can be followed for anaplastic level diffuse gliomas (Louis et al., 2016).

According to 2016 WHO and European Association for Neuro-Oncology (EANO) guidelines, investigations need to be performed as follows:

- IDH-status is evaluated by polymerase chain reaction (PCR) and direct sequencing; alternatively, immunohistochemistry (IHC) for IDH R132H is possible but negative cases need to be confirmed.
- ATRX loss and TP53 mutation are indirectly detected by IHC; their status is not required for the diagnosis, but it may be helpful to substantiate the diagnoses of IDH-mutant diffuse astrocytoma and anaplastic astrocytoma;

- 1p19q co-deletion is confirmed through a multilocus analysis, like Multiple Ligation-dependent Probe Amplification (MLPA);
- If IDH and 1p19q status are not available, the tumour is diagnosed as astrocytoma/anaplastic astrocytoma, NOS or oligodendroglioma/anaplastic oligodendroglioma, NOS or glioblastoma, NOS;
- H3K27M mutation can be detected by IHC using an antibody that recognizes the mutated protein or by PCR and direct sequencing.

Then other markers are evaluated to choose the appropriate treatment to administer to patients, like MGMT-promoter methylation status.

### 1.1.2 Therapy

*Targeted therapy: drugs on clinical trials*

NTRK inhibitors: ongoing trials are testing small-molecules tyrosin kinase inhibitors that block Trk activity. The most commonly studied drugs are Entrectinib and Larotrectinib, which display a significant antitumour activity with acceptable toxicity profile. Larotrectinib is a pan-Trk inhibitor with high specificity[34] and Entrectinib binds and inhibits TrkA, TrkB, TrkC, ROS1 and ALK[35].

Studies performed on gliomas and non-gliomas cases reported important findings: a small percentage of patients showed NTRK fusion as unique genetic alteration known, leading to a therapeutically relevant outcome in the future[36].

FGFR inhibitors: inhibitors of FGFR receptor are on clinical evaluation, one of them is Erdafitinib (JNJ-42756493), an oral ATP-competitive pan-FGFR selective inhibitor, which blocks tyrosine phosphorylation of activated FGFR. There are many other molecules that are under pre-clinical and clinical trials that, until now, are displaying good outcomes. The future is to develop new therapeutic strategies for IDH-WT patients which display a poor prognosis[37,38].

*Surgical resection, radio and chemotherapy*

Based on the localization of the gliomas, surgical resection is normally performed. After the resection, symptomatology generally disappears, with a good impact on patient quality of life. The depth of resection is done in order to preserve motor and intellective abilities, or at least, limiting the neurological damage.

AIOM 2016 guidelines[38] recommend an adjuvant chemotherapy and radiotherapy (STUPP protocol). As chemotherapeutic agent is administered TMZ, which is an alkylating agent that damages the double-helix of DNA, resulting in apoptosis of tumour cells.

## 1.2 Circumscribed gliomas

Circumscribed gliomas -pilocytic astrocytomas (PA), gangliogliomas (GG), ependymomas (EP) and dysembryoplastic neuro-epithelial tumours (DNET)- are mostly low-grade tumours but may progress to anaplasia[39]. These tumours have lower genetic complexity[40] than diffuse gliomas and therefore could be better candidate for targeted therapies, when complete surgical resection is not feasible.

### 1.2.1 Pylocitic Astrocytoma

Pilocytic astrocytomas are the most common glioma in children and adolescents, and affect males slightly more often than females (it accounts for 33.2% of all gliomas in the 0-14 years age group and 17.6% of all childhood primary brain tumours[41]). They are mainly located in the cerebellum and cerebral midline structures but can be found anywhere along the neuraxis; in the paediatric population, more tumours arise in the infratentorial region. Preferred sites include the optic nerve (optic nerve glioma), optic chiasm/hypothalamus, thalamus and basal ganglia, cerebral hemispheres, cerebellum, and brain stem and less frequently in the spinal cord[12].

They are generally circumscribed and slow-growing, and may be cystic. Pilocytic astrocytoma largely behaves as is typical of a WHO grade I tumour[12], and patients can be treated by surgical resection. However, complete resection may not be possible in some locations, such as the optic pathways and the hypothalamus. Pilocytic astrocytomas, particularly those involving the optic pathways, are a hallmark of neurofibromatosis type 1 (NF1).

In adults, pilocytic astrocytoma tends to arise about a decade earlier (mean patient age: 22 years) than does WHO grade II diffuse astrocytoma, but relatively few arise in patients aged > 50 years.

This astrocytic tumour of low to moderate cellularity often has a biphasic pattern, with varying proportions of compacted bipolar cells with Rosenthal fibres and loose-textured multipolar cells with microcysts. The biphasic pattern is best seen in cerebellar tumours. However, pilocytic astrocytoma can exhibit a wide range of tissue patterns, sometimes several within the same lesion. Although many pilocytic astrocytomas are benign, some show considerable hyperchromasia and pleomorphism. Rare mitoses are present, but brisk mitotic activity, in particular diffuse

brisk mitotic activity, characterizes anaplastic change, which has prognostic implications[42].

*Genetic profile*

The most frequent abnormality in pilocytic astrocytomas overall (found in > 70% of all cases) is an approximately 2 Mb duplication of 7q34, encompassing the BRAF gene. This is a tandem duplication resulting in a transforming fusion gene between KIAA1549 and BRAF[43]. The N-terminus of the KIAA1549 protein replaces the N-terminal regulatory region of BRAF, retaining the BRAF kinase domain, which is consequently uncontrolled and constitutively activates the MAPK pathway[43]. This abnormality is found at all anatomical locations, but is most frequent in cerebellar tumours and somewhat less common at other sites. The gene fusions involve nine different combinations of KIAA1549 and BRAF exons, making identification by RT-PCR or immunochemistry difficult, resulting in many centres accepting the demonstration of a duplication at 7q34 (usually using FISH probes) as evidence of the KIAA1549-BRAF fusion. In addition to harbouring BRAF fusion genes, essentially all pilocytic astrocytomas have been shown to have an alteration affecting some component of the MAPK pathway[44]. These alterations include the well-documented NF1 mutations, the hotspot BRAF mutation commonly known as the V600E mutation, KRAS mutations, alterations of NTRK-family receptor kinase genes and recurrent aberrations affecting the FGFR1; they include hotspot point mutations (N546K and K656E), FGFR1-TACC1 fusions similar to those seen in adult glioblastoma[45].

Concerning genetic susceptibility, pilocytic astrocytomas are the principal CNS neoplasm associated with neurofibromatosis 1 (NF1) and approximately 15% of individuals with NF1 develop pilocytic astrocytomas, particularly of the optic nerve pathways (optic pathway glioma), but other anatomical sites can also be affected. Conversely, as many as one third of all patients with a pilocytic astrocytoma of the optic nerve have NF1[12].

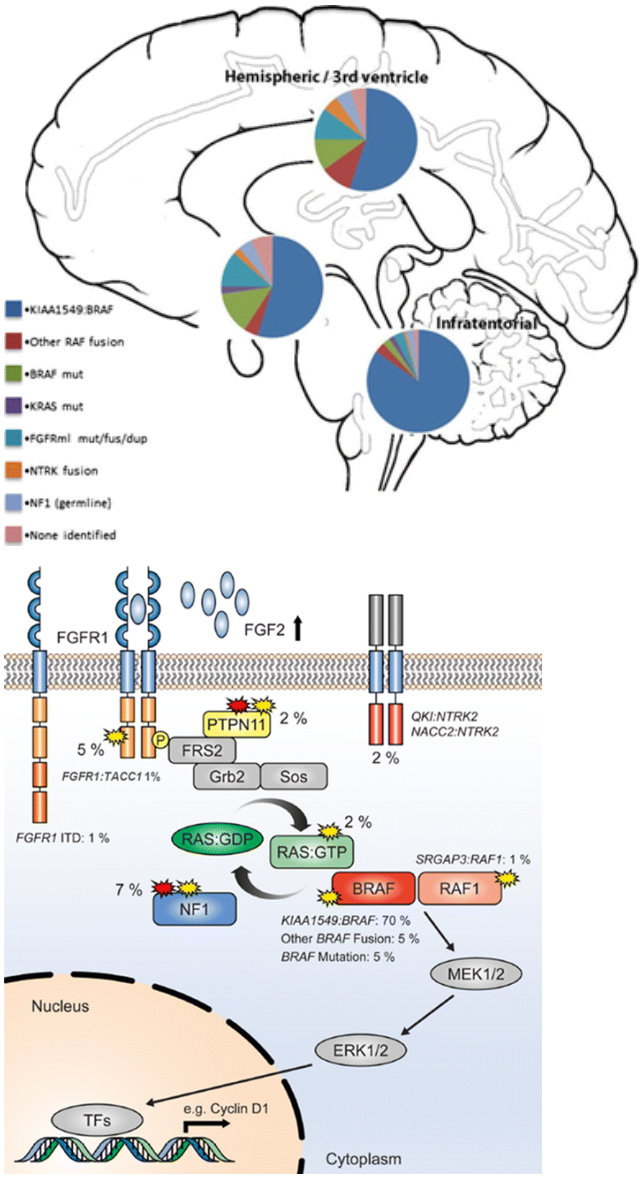


**Figure 3** Left: Estimated frequency of particular MAPK pathway alterations in different anatomic locations. Right: Summary showing the MAP kinase pathway with the approximate incidence of the different mutations in percent[46].

### 1.2.2 Ependymoma

Ependymomas are well-circumscribed tumours usually arising in or near the ventricular system or spinal canal, in the cerebral hemispheres, or at extra-CNS sites. Overall, 60% of the tumours develop in the posterior fossa, 30% in the supratentorial compartment, and 10% in the spinal canal [http://seer.cancer.gov/archive/csr/1975_2004].

Ependymomas can develop in patients of any age, with reported patient ages ranging from birth to 81 years [http://www.cbtrus.org]. However, incidence is greatly

dependent on histological variant, molecular group, and location. Posterior fossa ependymomas are most common among children, with a mean patient age at presentation of 6.4 years, and spinal tumours dominate a second age peak at 30-40 years. Supratentorial ependymomas affect paediatric as well as adult patients[12].

The 10-year overall survival (OS) is about 64% in pediatric patients and ranges from 70% to 89% in adult patients [http://www.cbtrus.org]. Tumours in infancy are associated with a particularly poor survival rate of only 42%– 55% at 5 years after diagnosis. The extent of surgical resection has for a very long time been the only clinical prognostic marker in EPN known to be associated with survival[47]. The current standard of care includes maximal safe surgical resection, followed by focal radiotherapy[47].

Classic ependymoma is a well-delineated glioma with monomorphic cells characterized by a variable density and round to oval nuclei with speckled nuclear chromatin. The key histological features are perivascular anucleate zones (pseudorosettes) and (true) ependymal rosettes; cell density can vary considerably in ependymoma.

A diagnosis of anaplastic ependymoma can be confidently made when an ependymal tumour shows a high cell density and elevated mitotic count alongside widespread microvascular proliferation and necrosis. Like the classic tumour, anaplastic ependymoma rarely invades adjacent CNS parenchyma to any significant extent. Traditionally, classic ependymoma and anaplastic ependymoma are considered to correspond histologically to WHO grades II and III, respectively. However, no association between grade and biological behaviour or survival has been definitively established[48].

### *Genetic profile*

Molecular alterations are very common in ependymoma and comprise cytogenetic, genetic, epigenetic, and transcriptomic changes. Ependymomas display a broad range of cytogenetic aberrations, most commonly gains of chromosomes 1q, 5, 7, 9, 11, 18, and 20 and losses of chromosomes 1p, 3, 6q, 6, 9p, 13q, 17, and 22[49,50].

Using DNA methylation profiling, several studies have provided support for the existence of distinct molecular groups among ependymomas[51,52]. In a large cohort (containing > 500 tumours), three groups were identified in each of the three CNS

compartments (i.e. supratentorial, posterior fossa, and spinal)[52]. Tumours with a subependymomatous morphology were classified into separate spinal (SP), posterior fossa (PF), and supratentorial groups (ST), called SP-SE, PF-SE, and ST-SE, respectively. Fusion genes involving either RELA or YAP1 characterize the other two supratentorial groups: ST-EPN-RELA and ST-EPN-VAP1. Supratentorial ependymomas are characterized by a recurrent structural variant, the C11orf95-RELA fusion gene, which is a by-product of chromothripsis and occurs in 70% of paediatric supratentorial ependymomas.

### 1.2.3 Ganglioglioma

Ganglioglioma is a well-differentiated, slow-growing glioneuronal neoplasm composed of dysplastic ganglion cells (i.e. large cells with dysmorphic neuronal features, without the architectural arrangement or cytological characteristics of cortical neurons) in combination with neoplastic glial cells. Gangliogliomas preferentially present in the temporal lobe (70% of cases) of children or young adults with early-onset focal epilepsy but these tumours can occur throughout the CNS, including brain stem, cerebellum, spinal cord, optic nerves, pituitary, and pineal gland[12,53].

BRAF V600E mutation occurs in approximately 25% of gangliogliomas, whereas IDH mutation or combined loss of chromosomal arms 1p and 19q exclude a diagnosis of a ganglioglioma. The prognosis is favourable, with a recurrence-free survival rate as high as 97% at 7.5 years[12].

In anaplastic gangliogliomas, malignant changes almost invariably involve the glial component and include increased cellularity, pleomorphism, and increased numbers of mitotic figures. Other potential anaplastic features include vascular proliferation and necrosis[54].

#### *Genetic profile*

BRAF V600E mutation is the most common genetic alteration in gangliogliomas, occurring in 20-60% of investigated cases[55,56]. This broad range of reported mutation frequency is probably related to the sensitivity of the detection methods used, as well as the patient age range in the investigated series, given that BRAF point mutations are particularly frequent in younger patients[57]. BRAF V600E is not specific for

gangliogliomas and it is also observed in other brain tumours, in particular pleomorphic xanthoastrocytomas, pilocytic astrocytomas, and dysembryoplastic neuroepithelial tumours[55,56]. V600E-mutant BRAF protein is localized mainly to ganglion cells, but can also be found in cells of intermediate differentiation, as well as in the glial compartment, suggesting that ganglion and glial cells in ganglioglioma may derive from a common precursor cell[57].

### 1.2.4 Dysembryoplastic neuroepithelial tumour (DNET)

DNET is a benign glioneuronal neoplasm typically located in the temporal lobe of children or young adults with early-onset epilepsy, predominantly with a cortical location and a multinodular architecture, and with a histological hallmark of a specific glioneuronal element characterized by columns made up of bundles of axons oriented perpendicularly to the cortical surface. These columns are lined by oligodendrocyte-like cells embedded in a mucoid matrix and interspersed with floating neurons. If only the specific glioneuronal element is observed, the simple form of DNET is diagnosed. Complex variants of DNET additionally contain glial tumour components, often with a nodular appearance. Long-term follow-up after epilepsy surgery shows an excellent outcome; recurrence or progression is exceptional[12].

*Genetic profile*

Paediatric DNETs have been shown to have stable genomes[58], whereas recurrent gains of whole chromosomes 5 and 7 were found in approximately 20% and 30% of cases, respectively, in a series of adult DNETs[59]. As in other glioneuronal tumours, recurrent BRAF V600E mutations were identified in 30% of DNETs. These mutations were associated with activation of mTOR signalling[60]. Neither TP53 mutations nor IDH1/IDH2 mutations or H3K27M mutations have been detected in DNETs[12]. Similarly, codeletion of whole chromosome arms 1p/19q has not been demonstrated in DNET[58,59].

## 1.3 NTRK genes

The tropomyosin receptor kinase (Trk) family comprises 3 transmembrane proteins named TrkA, TrkB and TrkC receptors that are encoded by neurotrophic tyrosine receptor kinase 1, NTRK1 (chromosome 1q23.1), NTRK2 (chromosome 9q21.33) and

NTRK3 genes (chromosome 15q25.3), respectively. Gene fusions involving NTRK genes encode chimeric Trk proteins with constitutively activated or overexpressed kinase function conferring oncogenic potential[61]. NTRK gene fusions are found in many human cancers including tumours of the CNS, mainly in high grade gliomas, referring to anaplastic astrocytomas, anaplastic oligodendrogliomas (both WHO grade III) and in GBMs (WHO grade IV)[62,63].

Trks are tyrosine kinases receptors expressed in human neuronal tissue and involved in development and function of the nervous system through activation by neurotrophins (NTs). Trks are structured with an extracellular ligand binding domain, a transmembrane region and an intracellular tyrosin kinase domain. The binding of the ligand to the receptor triggers the dimerisation of the receptors and phosphorylation of specific tyrosine residues in the intracytoplasmic kinase domain.

TrkA ligand is nerve growth factor (NGF) which activates MAPK pathway and ERK signalling (Figure 4). Otherwise this ligand-receptor interaction activates PLCγ and PI3K pathways. These are mechanisms that promote survival, differentiation, cell growth and preventing apoptosis[61].

TrkB is bound by brain-derived growth factor (BDGF), and NT-4 and NT-5 whereas TrkC couples NT-3. These latter receptors activate RAS/MAPK/ERK or PLCγ or PI3K pathways resulting in signal transduction pathways leading to proliferation, differentiation and survival (Figure 4)[63].

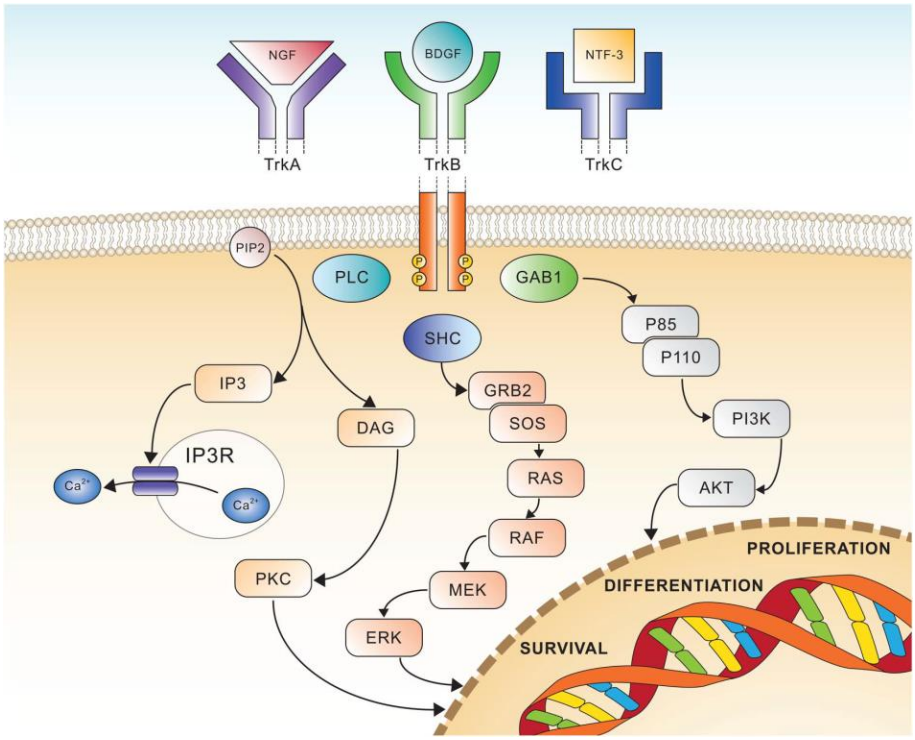


**Figure 4.** Schematic view of Trk receptors signalling, showing the three major pathways involved in cell differentiation, proliferation and survival[63].

NTRK translocations have been found in many tumours and involve the 3' region of the NTRK gene, which contains exons that encode the transmembrane domain (TM) and the tyrosine kinase domain (TK). The 3' region joins with a 5' sequence of a fusion partner gene by a chromosomal rearrangement. More precisely, the ligand binding domain is replaced by 5' fusion partner. When the fusion gene is transcribed, it gives rise to an oncogenic chimera that is a constitutively activated or overexpressed kinases[63].

NTRK gene fusion have been found initially in paediatric high grade gliomas with a recurrence of 40%[28] and have been demonstrated that NTRK3 is rearranged with ETS variant 6 (ETV6) gene (mapped on 12p13.2 and encoding for a transcription factor), while NTRK1 with tropomyosin 3 (TPM3) gene (located on chromosome 1q21.3), both these chimeric genes act as oncogenes[62]. Further studies demonstrated the presence of these translocations also in low grade pediatric gliomas and in adult high grade gliomas.

The gene fusions observed in high grade gliomas patients are:

- TPM3- NTRK1; NFASC-NTRK1; BCAN-NTRK1 in GBMs;

- AGBL4-NTRK2; VCAN-NTRK2; VCL-NTRK2 in GBMs;
- NACC2-NTRK2; QKI-NTRK2 in astrocytomas;
- ETV6-NTRK3; BTBD1-NTRK3 in GBMs.

All of them confers an oncogenic behaviour to fusion proteins[28].

NTRK gene fusions are common in children affected by diffuse intrinsic pontine glioma (DIPG)[28]. NTRK fusion genes in children <3 years old affected by high grade gliomas are associated to the paucity of additional mutations, and the rapid tumour onset, strongly suggest that these fusion genes are potent oncogenic drivers in early postnatal brain tumour development. Recently, the identification of NTRK fusions, also in other solid tumours, come into focus due to the availability of targeted therapies like NTRK inhibitors[63].

## 1.4 FGFR1 gene

FGFR genes control many biological functions, including cell proliferation, survival, and cytoskeletal regulation. FGFRs signaling is important during embryonal development of the CNS, and as a survival mechanism for adult neurons and astrocytes and promote self-renewal and fate specification of neural stem cells[64].

In many cancers, FGFRs aberrations have been implicated in tumour development and progression[65,66], and include FGFRs overexpression, amplification, mutations, splicing isoform variations, and FGFRs translocations[67]. While FGFRs genomic alterations have been identified in many solid tissue cancers, such events remain rare in glioblastoma (GBM)[68]. Nonetheless, FGFRs expression changes in astrocytes can lead to malignant transformation and GBM progression due to the activation of mitogenic, migratory, and antiapoptotic responses[69]. Of note, fusions between FGFRs and TACCs (transforming acidic coiled-coil containing proteins) genes were shown to be oncogenic in GBM[70], and occur in about 3% of GBM patients[68]. Whole-genome analyses of patient samples have revealed that the number of FGFRs mutations and amplifications are generally very low in GBM (FGFR1: 51/3068 samples, FGFR2: 12/2662; FGFR3: 16/2887; FGFR4: 9/2456; cancer.sanger.ac.uk).

Moreover, the expression of FGFR1 increases with WHO grade in astrocytomas, and increased FGFR1 levels in GBM are not due to amplification of the FGFR1 gene[64].

Functionally, FGFR1 expression in malignant glioma has been associated with increased migration of cancer cells[71]. In this study, a high expression of EPHA4 in glioma cells was found to potentiate FGF2–FGFR1 signaling and promoted cell growth and migration through the AKT/MAPK and RAC1/CDC42 pathways, respectively.

Loilome and colleagues[72] identified FGFR1 as a potential transducer of FGF2 effects on glioma cell proliferation, but whether other FGFRs also contribute was not directly tested. Nevertheless, the pharmacological inhibition of FGFRs signaling significantly reduced tumour cell growth in a range of established and patient-derived glioma lines. The malignancy-promoting effects of FGFR1 were further demonstrated in a study that found FGFR1 signaling promoting radioresistance in glioma cell lines through PLC1γ and HIF1α[73]. FGFR1 expression is regulated by the stem-cell associated transcription factor ZEB1, suggesting that FGFR1 may be associated with GBM cancer stem cells. A comprehensive analysis of the functions of FGFR1-3 in GBM found that FGFR1 indeed is preferentially expressed on GBM cancer stem cells, where it regulates the expression of the critical stem cell transcription factors SOX2, OLIG2, and ZEB1, thereby promoting tumourigenicity in vivo[74]. In summary, FGFR1 is a key regulator of tumour growth, invasion, therapy resistance, and cancer stemness in malignant glioma.

# 2. AIM OF THE STUDY

Since midline gliomas are one of the more aggressive tumours of CNS and generally unresectable, the aim of this study is to contribute to unravel the genomic landscape of this heterogeneous group of gliomas in order to better define the prognostic value of molecular biomarkers and identify new therapeutic strategies that could improve patient care. Recently, a new class of tyrosine kinase inhibitors has been introduced in clinical trials. For this reason, we investigated the presence of FGFR1 mutations and NTRK gene rearrangements in order to explore the frequency, the possible correlation with clinical, histologic and genomic features and also the feasibility of testing in the diagnostic routine analysis to allow a possible future use of targeted therapies in clinical practice.

Moreover, since there is a scant literature about FGFR1 mutation rate in rarer CNS tumours like pilocytic astrocytoma, ganglioglioma, dysembryoblastic neuroepithelial tumour and ependymoma and also specific inhibitors are available in clinical trials, our idea is to investigate these mutational hotspots in a cohort of circumscribed gliomas. This information could be helpful in defining different therapeutic strategies when surgery is not feasible.

# 3. MATERIAL AND METHODS

## 3.1 Sample collection

### 3.1.1. Midline Gliomas

Patients (>15 years) with diagnosis of MLG were retrospectively identified from each institution's databases (OncoNeuroTek tumour bank, GH Pitié-Salpêtrière, (Paris, France) and AOU Maggiore della Carità, SCDU Anatomia Patologica (Novara, Italy)) between 1996 – 2017 for the French cohort and from 1993 to 2017 for the Italian cohort. For two patients (Italian cohort) the primary tumour and the recurrent tumour were collected.

Inclusion criteria were as follows:

(1) tumour arising in midbrain location (thalamus, hypothalamus, pineal region, brainstem, cerebellum or spinal cord), verified on neuroimaging at diagnosis;

(2) histopathological confirmation of diffuse glioma according to WHO 2016 classification;

(3) available follow-up data.

All tumour samples underwent histopathological review.

The French cohort has been analyzed previously[75] to the Italian one and it has been considered as a starting point for subsequent analyses.

### 3.2.1 Circumscribed gliomas

Patients (>15 years) with diagnosis of pilocytic astrocytoma (PA), ganglioglioma (GG), dysembryoblastic neuroepithelial tumour (DNET) and ependymoma (EP) were retrospectively identified from each institution's databases (Onconeurotek tumour bank GH Pitié-Salpêtrière, (Paris, France), and "AOU Maggiore della Carità, SCDU Anatomia Patologica (Novara, Italy)) according to the histopathological diagnosis. All tumour samples underwent histopathological review.

All tumour samples and clinical data were collected in accordance with the tenets of the Declaration of Helsinki.

## 3.2 Tissue microarray

Tissue microarray (TMA) technique allow to handle up to several samples in one block or in one slide as it may contain hundreds of small different and representative tissue samples on a single paraffin block. These samples are obtained by the extraction of a tissue core of 1.5 mm of diameter, by using a holed needle, from “donor blocks” and re-embedded all together in a single empty block, called “recipient block”, at defined coordinates. In the array are also put other tissues (like liver) as references for the orientation of the array.

At first, haematoxylin-eosin (H&E) stained slides of each sample that will be included in the TMA are required to select the most significant tumour areas avoiding normal brain tissue, necrosis or haemorrhagic regions. For each sample, 1 to 3 areas have been selected for TMA construction by marking on the H&E slide, depending on the extension of the tumour area. The marked H&E slide is necessary for the alignment of the selected areas to the corresponding FFPE block. The alignment is done through a PC connected to the instrument TMA Master (3DHISTECH LTD) and the software used is TMA Master 1.14 SP3 (3DHISTECH LTD). After that, the same instrument takes tissue cores from FFPE samples (donor blocks), and then all the cores are re-embedded in one single recipient block.

TMA was constructed only for midline gliomas belonging to the Italian cohort. In our recipient block are present 107 samples cores and 8 liver cores used as orientation references.

TMA construction was performed by the team of Dr. Milo Frattini at Istituto Cantonale di Patologia (Locarno, Switzerland).

For the following steps, 4 µm sections from the recipient block are cut using the microtome and put on a positively charged glass slide in order to perform FISH analysis and immunohistochemistry stainings.

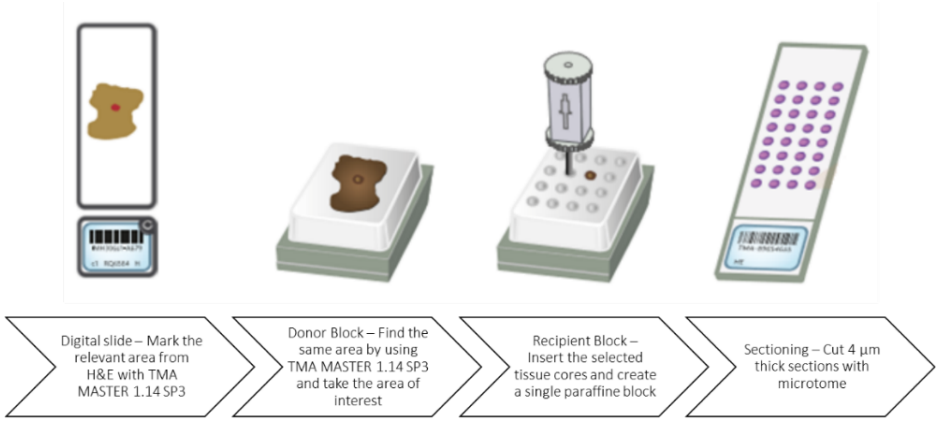


**Figure 5.** Schematic description of TMA technique.

## 3.3 DNA extraction and quantification

Genomic DNA of GH Pitié-Salpêtrière's cases was extracted from formalin-fixed paraffin-embedded (FFPE) or frozen samples, as previously described[75]. Genomic DNA of patients from Maggiore della Carità Hospital were extracted from five 5µm sections of FFPE samples by the GeneRead DNA FFPE Kit (Qiagen) on the QIAcube automatic extractor (Qiagen) according to the manufacturer's protocol.

## 3.3 Sanger sequencing

Hotspot mutation regions of IDH1 (codon 132), IDH2 (codon 172), TERT promoter (positions -250 and -228), FGFR1 exons 12 (codon 546) and 14 (codon 656), H3F3A (codons 27 and 34), HIST1H3B (codon 27) and BRAF exon 15 (codon 600) were amplified by standard PCR amplification and sequenced by Sanger sequencing. Primer sequences are reported in Table 1.

| Gene | | Sequence 5'-->3' |
|---|---|---|
| IDH1 | Forward | TGTGTTGAGATGGACGCCTATTTG |
| | Reverse | TGCCACCAACGACCAAGTCA |
| IDH2 | Forward | GCCCGGTCTGCCACAAAGTC |
| | Reverse | TTGGCAGACTCCAGAGCCCA |
| H3F3A | Forward | GTGATCGTGGCAGGAAAAGT |
| | Reverse | CAAGAGAGACTTTGTCCCATTTT |
| HIST1H3B | Forward | GTTTTGCCATGGCTCGTACT |
| | Reverse | AAGCGAAGATCGGTCTTGAA |
| FGFR1 exon 12 | Forward | CCTCCTCCCTTCCCAAGTAA |
| | Reverse | GGACTGATACCCCAGCTCAG |
| FGFR1 exon 14 | Forward | CTTCCAGCTCCCTCACCTC |
| | Reverse | CCCACTCCTTGCTTCTCAGAT |
| TERT promoter | Forward | TCCTGCCCCTTCACCTT |
| | Reverse | AGCACCTCGCGGTAGTGG |
| BRAF | Forward | TGCTTGCTCTGATAGGAAAATG |
| | Reverse | CAGGATCTCAGGGCCAAAAAT |

**Table 1.** Primers' sequences

All PCR amplifications were performed at 3 minutes at 94°C; 35 cycles at 94°C 15 seconds, 60°C 45 seconds, 72°C 1 minute, with a final step at 72°C for 8 minutes.

PCR reactions were set up with AmpliTaq Gold 360 MasterMix (Thermo Fisher) 1x, 500nM of each primer and only for TERT promoter amplification, 10% 360 GC enhancer (Thermo Fisher).

Sequencing reactions were performed with BigDye Terminator v.1.1 (Thermo Fisher) and analysed on the sequencer 3130 Genetic Analyser (Applied Biosystems).

## 3.4 Fluorescence *in situ* hybridization (FISH)

FISH analyses were perfomed by using NTRK1, NTRK2 and NTRK3 break-apart probes (Zyto*Light* SPEC Dual Color Break Apart probes, ZytoVision).

NTRK1 probe is a mixture of two direct labelled probes hybridizing to the 1q22-q23.1 band (Figure 6). The green fluorochrome direct labelled probe hybridizes proximal and the red fluorochrome direct labelled probe hybridizes distal to the NTRK1 gene.

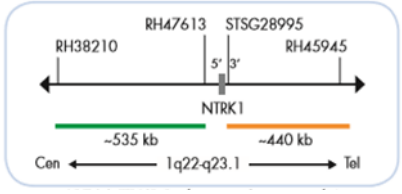

**Figure 6.** NTRK1 probe map (not to scale).

NTRK2 probe is a mixture of two direct labelled probes hybridizing to the 9q21.32-q21.33 band (Figure 7). The green fluorochrome direct labelled probe hybridizes proximal to the NTRK2 breakpoint region at 9q21.32-q21.33, the red fluorochrome direct labelled probe hybridizes distal to the NTRK2 breakpoint region at 9q21.33.

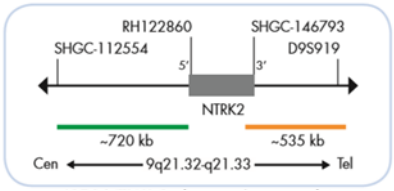


**Figure 7.** NTRK2 probe map (not to scale).

NTRK3 probe is a mixture of two direct labelled probes hybridizing to the 15q25.3-q26.1 band (Figure 8). The orange fluorochrome direct labelled probe hybridizes proximal to the NTRK3 breakpoint region at 15q25.3, the green fluorochrome direct labelled probe hybridizes distal to the NTRK3 breakpoint region at 15q25.3-q26.1.

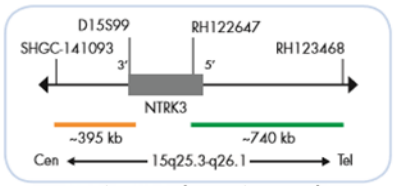


**Figure 8.** NTRK3 probe map (not to scale).

The result interpretation is equal for all the 3 probes. If there is a translocation, the 2 fluorescent signals (green and red) are separated and there are 2 distinct colours coupled with a fusion signal corresponding to the wild-type allele. If there is no translocation the 2 signals appear as a fusion signal, for a total of 2 fusion signals/cell.

## FISH protocol

4 µm thick sections of the FFPE tissue or TMA need to be cut and put on polarized (positively charged) slides. For each patient or TMA, 3 sections were cut, 1 for each gene analysis (NTRK1, NTRK2 and NTRK3).

***Deparaffination***: slides are incubated into a dry heat oven at 60°C overnight (ON). The day after, tissues are re-hydrated through xylene and decreasing alcoholic series (10' xylene, 10' xylene, 5' 100% alcohol, 5' 95% alcohol, 5' 80% alcohol, 5' 75% alcohol, 5' deionized water).

***Pretreatment***: incubation in pre-heated Heat Pretreatment Solution (Zyto*Light* FISH-Tissue Implementation Kit, ZytoVision) at 92°C for 20'. Then the slides are brought to

room temperature (RT) in deionized water for 5'. Subsequently, the slides are air-dried.

***Tissue digestion***: incubation with Pepsin Solution (Zyto*Light* FISH-Tissue Implementation Kit, ZytoVision) is performed for 4'-7' at 37°C in a hybridizer (TopBrite™, Resnova) with humidity chamber. After that slides are washed in Wash Buffer SSC (*ZytoLight* FISH-Tissue Implementation Kit, ZytoVision) for 5' at RT and then 5' in deionized water. Tissues are dehydrated (1' 75% alcohol, 1' 80% alcohol, 1' 95% alcohol, 1' 100% alcohol), then DAPI and coverslips are applied, and tissue digestion is checked by fluorescence microscope. If the tissue is digested enough (only nuclei are visible without cytoplasm and membranes) DAPI and coverslips are removed with Wash Buffer SSC (Zyto*Light* FISH-Tissue Implementation Kit, ZytoVision) for 5' at RT and 5' in deionized water. Since the probes used are hydrophobic, it is necessary to dehydrated through increasing alcoholic series (1' 75% alcohol, 1' 80% alcohol, 1' 95% alcohol, 1' 100% alcohol). Then sections are air-dried.

***Probe hybridization***: 5 µl of each probe are applied for each section (protecting from light) coverslip is applied and sealed with Fixo-gum (Marabu, Germany) to keep the probe on the section and avoid its evaporation. Glass slides are put into the hybridizer (TopBrite™) with humidity chamber and denaturated for 10' at 75°C and then hybridized at 37°C ON.

***Stringency washes and mounting***: the day after, coverslips are removed and stringency washes are performed with 1X Wash Buffer SSC (Zyto*Light* FISH-Tissue Implementation Kit, ZytoVision), 2x5'at 37°C. Then tissues are dehydrated (1' 75% alcohol, 1' 80% alcohol, 1' 95% alcohol, 1' 100% alcohol), air-dried and counterstained with DAPI. FISH are ready and fluorescence can be detected through fluorescence microscope.

***Fluorescence acquisition***: fluorescent signals were acquired by using the Axioplan2 microscope (Zeiss) coupled with AxioCam HRm (Zeiss) camera and AxioVision software (Zeiss) for images acquisition. We acquired 3 fluorescences (FITC, Rhodamine and DAPI channels) for each high-power field at 63x (oil immersion). For each sample, we analysed at least 6 high-power fields and a minimum of 100 cells for each case across all the respective cores in the TMA.

Up to now, there are not present any guidelines that establish a specific cut-off (% positive cells) for NTRK rearrangements. We considered as positive, cases with any percentage of positive cells; positivity is considered when contiguous cells report a signal pattern consisting of one orange/green fusion signal, one separate orange signal and one separate green signal (ZytoVision).

## 3.5 Immunohistochemistry

ATRX expression analysis in samples of the Italian cohort were performed by immunohistochemistry on a Ventana BenchMark ULTRA automated platform (Roche Diagnostics) coupled with ultraView Universal DAB Detection Kit (Ventana Medical Systems – Roche). A rabbit polyclonal antibody (HPA001906, Sigma-Aldrich) was used at 1:400 dilution, 90' antigen retrieval with CC1 buffer (Ventana Medical Systems – Roche), 60' antibody incubation and signals were amplified with the Amplification kit (Ventana Medical Systems – Roche).

## 3.6 Other analyses

Cases belonging to the French cohort of MLG were previously analysed for ATRX and p53 nuclear expression by immunohistochemistry, CDKN2A/p16 loss and EGFR amplification at GH Pitié-Salpêtrière (Paris)[75].

## 3.7 Statistical analysis

Continuous variables have been described with mean and standard deviation, categorical variables with counts and percentages. The distributions of the categorical variables within the groups were analysed with the chi-square test or with the Fisher exact test.

The distributions of continuous variables within the groups of interest were analysed with the independent t-student test.

The survival curves were obtained according to the Kaplan Meier method and were compared with the log-rank test.

P-values $<0.05$ were considered statistically significant. All the analyses were performed with the STATA15 software.

# 4. RESULTS

## 4.1 Molecular characteristics of French and Italian cohort of midline gliomas

Patients characteristics and tumour main molecular alterations, according to the location are reported in Table 2.

The two cohorts showed different distribution in the location of the tumour as well as in the percentage of H3F3A mutations. In the French cohort, histone H3K27M mutation was found in 38/110 patients (34%) and was significantly associated with a younger age at diagnosis (median 33 years vs. 53 years, $p=6*10^{-5}$). In Italian cohort, H3F3A mutations were identified in 20% of cases and there was not seen any association with a younger age, probably due to the lower number of mutated cases. H3K27M mutation were mutually exclusive with IDH1, and inversely associated with TERTp mutation in both cohorts. H3K27M was found in all the locations but was significantly associated with thalamic and spinal locations in French cases; this evaluation did not reach any statistically significant differences in the Italian cohort due to the low number of mutated cases (Table 3).

In the French cohort, IDH1 mutations were found in 6 patients (1 grade II, 4 grade III, 1 grade IV) out of 102: strikingly, all 6 IDH1 mutated tumours were located in brainstem (6/24 vs. 0/78 for MLG not involving the brainstem; $p=7.5.10^{-5}$). Noteworthy, only one out of the 5 IDH1 mutation identified by sequencing was IDH1 p.Arg132His (R132H), the other mutations were p.Arg132Gly (R132G), p.Arg132Cys (R132C), p.Arg132Leu (R132L), p.Arg132Gly (R132G), which contrasted with non-midline IDH1-mutant gliomas. Also in the Italian cohort is present a non-canonincal IDH1 mutation (R132G) in two cases (astrocytoma grade II of the ventricle) belonging to the same patient (primary and recurrent tumour).

According to the 2016 WHO classification, all H3K27M mutated MLG were considered as grade IV tumours. However, we did not find any impact of histone H3K27M mutation in terms of overall survival in both cohort. Analysing the impact of specific alterations on survival, the French cohort showed that IDH1 mutation, loss of ATRX and FGFR1 mutations were associated with longer survival while the Italian cohort did not show any statistically significant differences within these gene alterations, probably due to the lower number of cases, but only with a poor survival in pTERT mutated cases (Figure 9, also reported in the French cohort).

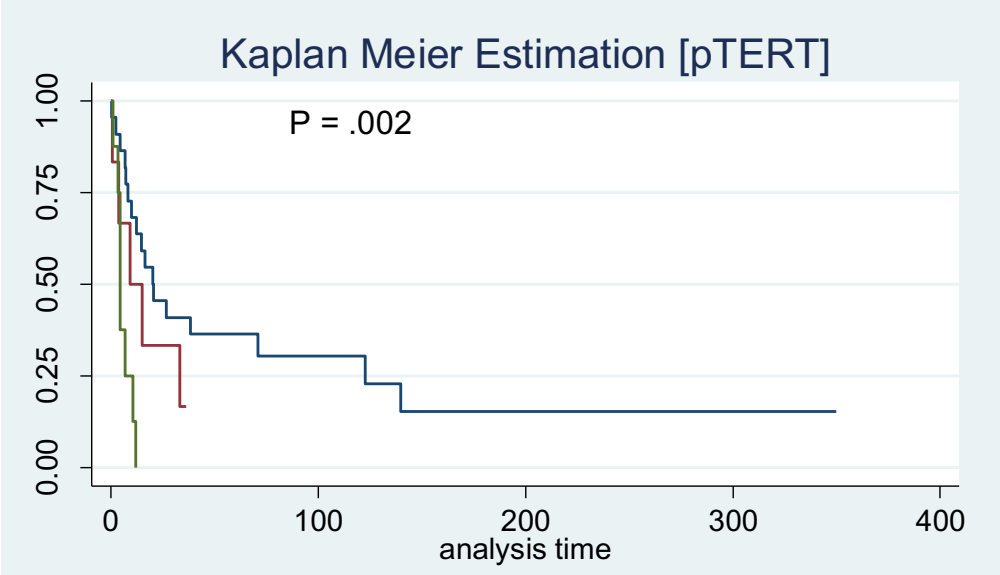


**Figure 9.** Kaplan Meier curve of pTERT mutated vs wild-type cases (Italian cohort). The red line represents the C228T mutation, the green line the C250T mutation and the blue line the wild-type cases.

*FGFR1 mutation analysis*

Recurrent FGFR1 mutations affecting two hotspots were identified in 18% of patients (13/73) in the French cohort: p.Asn546Lys (9), p.Asn546Asp (2), p.Lys656Glu (2) with diverse locations: 7/37 thalamus (19%), 2/12 brainstem (17%), 2/13 cerebellar (15%), 1/3 spinal cord (33%) (p=0.9), in both H3K27M MLG (6/23) and histone wild-type MLG (6/45); p=0.3; 6/41 IDH wildtype vs. 0/4 IDH mutated, p=1. In order to investigate whether FGFR1 mutation were specific to midline diffuse gliomas, we sequenced from OncoNeuroTek tumour bank 479 DNA samples extracted from unselected hemispheric gliomas (170 GBM, 151 grade III, 157 grade II; of which, 197 were IDH mutated, 212 IDH wild type, and 70 undetermined) for the presence of FGFR1 mutations: we found only one mutation in a patient with an IDH wildtype GBM involving the corpus callosum, suggesting that FGFR1 mutations are restricted to midline diffuse gliomas (13/73 vs. 1/479; $p=1.2.10^{-10}$). This data were further confirmed by public data (http://www.cbioportal.org): out of 1722 patients with diffuse gliomas, only 2 patients had FGFR1 activating mutation (13/73 vs. 2/1722; $p=10^{-16}$): one GBM with K656E mutation but no clinical information on location and one 1p/19q-codeleted IDH1 mutant frontal oligodendroglioma with N546K mutation. In the Italian cohort, FGFR1 mutations were found only in 3/46 cases (7%), all p.Lys656Glu mutations (1 GBM-H3K27M of the III ventricle, 1 anaplastic

oligodendroglioma-H3K27M of the parasellar region and 1 intramedullary anaplastic astrocytoma). These cases were wild-type for IDH1/2, TERT promoter and BRAF, while 2 out of 3 cases were H3F3-K27M mutated.

| | French Cohort | | | | | | Italian Cohort | | | | | |
|---|---|---|---|---|---|---|---|---|---|---|---|---|
| | **Total** | **Non-thalamic diencephalic** | **Thalamic** | **Brainstem** | **Cerebellar** | **Spinal cord** | **Total** | **Non-thalamic diencephalic** | **Thalamic** | **Brainstem** | **Cerebellar** | **Spinal cord** |
| **N, % (n)** | **116** | 4 (4/116) | 48 (57/116) | 26 (30/116) | 15 (17/116) | 7 (8/116) | **46** | 27/46 | 5/46 | 1/46 | 5/46 | 8/46 |
| **Sex ratio (M/F)** | **1.58 (71/45)** | 3 (3/1) | 1.38 (33/24) | 2.33 (21/9) | 1.13 (9/8) | 1.67 (5/3) | **1.71 (29/17)** | 2 (18/9) | 0.7 (2/3) | 1 (1/0) | 1.5 (3/2) | 1.67 (5/3) |
| **Age at surgery in years, median (range)** | **46.5 (15 – 75)** | 55.5 (46 - 66) | 49 (15 - 75) | 41.5 (22 - 75) | 50 (23 - 73) | 34.5 (18 - 57) | **46 (16-81)** | 45 (21-69) | 51 (28-69) | 17 | 49 (24-81) | 49 (17-63) |
| **Histology according to 2016 WHO classification, % (n)** | | | | | | | | | | | | |
| **Grade II** | **10 (12/116)** | **0** | **12 (7/57)** | **13 (4/30)** | **6 (1/17)** | **0 (0/8)** | **24 (11/46)** | **26 (7/27)** | **20 (1/5)** | **0** | **0** | **38 (3/8)** |
| diffuse astrocytoma, IDH mutant | 1 (1/116) | 0 | 0 (0/57) | 3 (1/30) | 0 | 0 | 4 (2/46) | 7 (2/27) | 0 | 0 | 0 | 0 |
| diffuse astrocytoma, IDH wild type | 6 (7/116) | 0 | 11 (6/57) | 3 (1/30) | 0 | 0 | 20 (9/46) | 19 (5/27) | 20 (1/5) | 0 | 0 | 38 (3/8) |
| diffuse astrocytoma, NOS | 3 (3/116) | 0 | 2 (1/57) | 3 (1/30) | 6 (1/17) | 0 | 0 | 0 | 0 | 0 | 0 | 0 |
| oligodendroglioma, IDH mutant and 1p/19q codeleted | 0 | 0 | 0 | 0 | 0 | 0 | 0 | 0 | 0 | 0 | 0 | 0 |
| oligodendroglioma, NOS | 0 | 0 | 0 | 0 | 0 | 0 | 0 | 0 | 0 | 0 | 0 | 0 |
| oligoastrocytoma, NOS | 1 (1/116) | 0 | 0 | 3 (1/30) | 0 | 0 | 0 | 0 | 0 | 0 | 0 | 0 |

| | | | | | | | | | | | | |
|---|---|---|---|---|---|---|---|---|---|---|---|---|
| **Grade III** | **15 (17/116)** | **0** | **9 (5/57)** | **33 (10/30)** | **0** | **25 (2/8)** | **17 (8/46)** | **22 (6/27)** | **40 (2/5)** | **0** | **40 (2/5)** | **38 (3/8)** |
| anaplastic astrocytoma, IDH mutant | 3 (4/116) | 0 | 0 | 13 (4/30) | 0 | 0 | 2 (1/46) | 4 (1/27) | 0 | 0 | 0 | 0 |
| anaplastic astrocytoma, IDH wild type | 8 (9/116) | 0 | 7 (4/57) | 13 (4/30) | 0 | 13 (1/8) | 15 (7/46) | 15 (4/27) | 20 (1/5) | 0 | 40 (2/5) | 38 (3/8) |
| anaplastic astrocytoma, NOS | 3 (3/116) | 0 | 0 | 7 (2/30) | 0 | 13 (1/8) | 0 | 0 | 0 | 0 | 0 | 0 |
| anaplastic oligodendroglioma, IDH mutant and 1p/19q codeleted | 0 | 0 | 0 | 0 | 0 | 0 | 0 | 0 | 0 | 0 | 0 | 0 |
| anaplastic oligodendroglioma, NOS | 0 | 0 | 0 | 0 | 0 | 0 | 4 (2/46) | 4 (1/27) | 20 (1/5) | 0 | 0 | 0 |
| anaplastic oligoastrocytoma, NOS | 0 | 0 | 0 | 0 | 0 | 0 | 0 | 0 | 0 | 0 | 0 | 0 |
| high grade glioma in NF1 | 1 (1/116) | 0 | 2 (1/57) | 0 | 0 | 0 | 0 | 0 | 0 | 0 | 0 | 0 |
| **Grade IV** | **75 (87/116)** | **100 (4/4)** | **79 (45/57)** | **53 (16/30)** | **94 (16/17)** | **75 (6/8)** | **48 (22/46)** | **52 (14/27)** | **40 (2/5)** | **1** | **60 (3/5)** | **25 (2/8)** |
| glioblastoma, IDH mutant | 1 (1/116) | 0 | 0 | 3 (1/30) | 0 | 0 | 0 | 0 | 0 | 0 | 0 | 0 |
| glioblastoma, IDH wild type | 37 (43/116) | 0 | 37 (21/57) | 20 (6/30) | 76 (13/18) | 0 | 48 (22/46) | 52 (14/27) | 40 (2/5) | 1 | 60 (3/5) | 25 (2/8) |
| glioblastoma, NOS | 2 (2/116) | 75 (3/4) | 2 (1/57) | 0 | 6 (1/17) | 0 | 0 | 0 | 0 | 0 | 0 | 0 |
| **Diffuse midline glioma, H3 K27M mutant** | **35 (41/116)** | **25 (1/4)** | **40 (23/57)** | **30 (9/30)** | **12 (2/17)** | **75 (6/8)** | **20 (9/46)** | **4** | **1** | **1** | **0** | **3** |

| **Median OS in months (95% CI)** | **17.3 months (14.5 – 23.8 months)** | 8.2 months (0.3 - NA months) | 17.3 months (14.5 – 27.5 months) | 16.3 months (11.6 – 52.2 months) | 19.7 months (8.3 – NA months) | 23.0 months (3.8 – NA months) | 43.7 months | 34.6 months | 39.7 months | 6.8 months | NA | 49 months |
|---|---|---|---|---|---|---|---|---|---|---|---|---|
| **IDH mutation, % (n)** | **6 (6/102)** | 0 | 0 | 25 (6/24) | 0 | 0 | **9 (4/46)** | 12 (3/27) | 0 | 0 | 0 | 0 |
| **IDH1** | 100 (6/6) | 0 | 0 | 100 (6/6) | 0 | 0 | 100 (4/4) | 100 (3/3) | 0 | 0 | 0 | 0 |
| **IDH2** | 0 | 0 | 0 | 0 | 0 | 0 | 0 | 0 | 0 | 0 | 0 | 0 |
| **K27M mutation, % (n)** | **34 (38/111)** | 25 (1/4) | 40 (22/55) | 29 (8/28) | 12 (2/17) | 71 (5/7) | **20 (9/46)** | 15 (4/27) | 20 (1/5) | 100 (1/1) | 0 | 38 (3/8) |
| **H3F3A** | 79 (30/38) | 100 (1/1) | 86 (19/22) | 37 (3/8) | 100 (2/2) | 100 (5/5) | 100 (9/9) | 100 (4/4) | 100 (1/1) | 100 (1/1) | 0 | 100 (3/3) |
| **HIST1H3B** | 3 (1/38) | 0 | 0 | 13 (1/8) | 0 | 0 | 0 | 0 | 0 | 0 | 0 | 0 |
| **NA (IHC only)** | 18 (7/38) | 0 | 14 (3/22) | 50 (4/8) | 0 | 0 | 0 | 0 | 0 | 0 | 0 | 0 |
| **ATRX loss, % (n)** | **19 (16/86)** | 0 | 16 (7/45) | 30 (6/20) | 17 (2/12) | 20 (1/5) | **20 (9/46)** | 19 (5/27) | 40 (2/5) | 0 | 40 (2/5) | 0 |
| **pTERT mutation, % (n)** | **37 (32/86)** | 66 (2/3) | 40 (19/47) | 38 (6/16) | 23 (3/13) | 29 (2/7) | **35 (16/46)** | 37 (10/27) | 60 (3/5) | 0 | 40 (2/5) | 1 |
| **C228T:** | 78 (25/32) | 100 (2/2) | 74 (14/19) | 83 (5/6) | 67 (2/3) | 100 (2/2) | 50 (8/16) | 80(8/10) | 0 | 0 | 0 | 0 |
| **C250T:** | 25 (8/32) | 0 | 25 (5/19) | 33 (2/6) | 33 (1/3) | 0 | 50 (8/16) | 20 (2/10) | 100 (3/3) | 0 | 100 (2/2) | 100 (1/1) |
| **FGFR1 mutation, % (n)** | **19 (13/70)** | 0 | 18 (7/38) | 23 (3/13) | 15 (2/13) | 33 (1/3) | **7 (3/46)** | 7 (2/27) | 0 | 0 | 0 | 12 (1/8) |
| **EGFR amplification, % (n)** | **12 (7/57)** | NA | 11 (3/28) | 10 (2/20) | 40 (2/5) | 0 | NA | NA | NA | NA | NA | NA |
| **p16/CDKN2A loss, % (n)** | **19 (11/57)** | NA | 21 (6/28) | 15 (3/20) | 40 (2/5) | 0 | NA | NA | NA | NA | NA | NA |
| **BRAF V600E mutation, % (n)** | **0** | 0 | 0 | 0 | 0 | 0 | **2 (1/46)** | 0 | 20 (1/5) | 0 | 0 | 0 |

**Table 2**. Patients characteristics and tumour main molecular alterations, according to the location.

| | French Cohort | | | Italian Cohort | | |
|---|---|---|---|---|---|---|
| | **K27M wild type** | **K27M mutated** | **P-value** | **K27M wild type** | **K27M mutated** | **P-value** |
| **N** | 73 | 38 | NA | 37 | 9 | |
| **Sex ratio (M/F)** | 1.52 (44/29) | 1.53 (23/15) | 0.98 | 1.64 (23/14) | 2 (6/3) | 0.58 |
| **Age at surgery in years, median (range)** | 53 (23 – 75) | 33 (15 – 65) | **<0.0001** | 48 (17-81) | 39 (16-69) | 0.11 |
| **Location, % (n)**<br>- **Non-thalamic diencephalic**<br>- **Thalamic**<br>- **Brainstem**<br>- **Cerebellar**<br>- **Spinal cord** | <br>4 (3/73)<br>45 (33/73)<br>27 (20/73)<br>21 (15/73)<br>3 (2/73) | <br>3 (1/38)<br>58 (22/38)<br>21 (8/38)<br>5 (2/38)<br>13 (5/38) | **0.04** | <br>62 (23/37)<br>11 (4/37)<br>0<br>13.5 (5/37)<br>13.5 (5/37) | <br>44 (4/9)<br>11 (1/9)<br>11 (1/9)<br>0<br>33 (3/9) | 0.12 |
| **Median OS in months** | 15.0 months | 18.6 months | 0.65 | 51.7 months | 17.2 months | 0.59 |
| **IDH mutation, % (n)** | 17 (5/30) | 0 | 0.16 | 11 (4/37) | 0 | 0.49 |
| **ATRX loss, % (n)** | 15 (8/54) | 26 (8/31) | 0.25 | 22 (8/37) | 11 (1/9) | 0.47 |
| **pTERT mutation, % (n)**<br>- **C228T:**<br>- **C250T:** | 52 (27/52)<br>20<br>7 | 19 (5/27)<br>4<br>1 | **0.007** | 44 (16/37)<br>8<br>8 | 0 | **0.027** |
| **FGFR1 mutation, % (n)** | 13 (6/46) | 26 (6/23) | 0.19 | 3 (1/37) | 22 (2/9) | 0.11 |
| **BRAF mutation, % (n)** | 0 | 0 | NA | 3 (1/37) | 0 | 1.00 |

**Table 3.** Clinical, histological and molecular characteristics in patients with H3K27M versus H3K27wt MLG

## 4.2 NTRK gene analysis in MLG

### 4.2.1 NTRK1 status

The Italian cohort of MLG was investigated for NTRK genes rearrangements.

In five cases out of 45 (11.1%) the analysis failed due to tissue artifacts (pre-analytical problems).

NTRK translocations were detected in 6 (15%) cases. Concerning case 2, we have selected and analysed primary (case 2A) and recurrent (case 2B) tumours. For statistical analysis the case number 2 were considered as a single case.

Clinical and genomic profiling of the 6 translocated reported: 4 (66,7%) males and 2 (33.3%) females, 43 year as mean age of diagnosis, 2 (33.3%) cases localized in lateral ventricle, 1 (16.67%) in thalamus, 1 (16.67%) in brainstem, 1 (16.67%) involving corpus callosum and 1 (16.67%) in spinal cord. Two cases (33.3%) were histological diagnosed as grade II astrocytoma (according to 2016 WHO classification) and 4 (66,7%) cases as GBMs. Five cases (83.3%) did not show IDH1 mutations, 1 case (16.67%) harbour R132G mutation in IDH1. None IDH2 mutations were identified. In one case (16.67%) G34R and R26H mutations were present in H3F3A gene, 2 (33.3%) cases showed K27M mutation in H3F3A and 3 (50%) cases were WT. All cases (100%) did not show mutations in HIST1H3B, FGFR1 (exon 12 and 14) and BRAF (exon 15). One case (16.67%) harboured pTERT C250T mutation, 1 case (16.67%) showed C228T and 4 cases (66,7%) were WT. Concerning ATRX status, 3 cases (50%) showed protein loss and in 3 cases (50%) ATRX expression is retained in the nucleus.

Regarding NTRK1, the percentages of cells showing NTRK1 translocation were: 38% in case 1, 29% and 20% respectively in case 2A and 2B, 25% in case 3, 29% in case 4, 34% in case 5 and 17% in case 6.

In Table 4, detailed genomic profiling and protein expression of the 6 translocated cases are shown.

| Case | Gender | Tumour | Age at diagnosis | Localization | Diagnosis | IDH1 | IDH2 | H3F3A | HIST1H3B | FGFR1 ex. 12 | FGFR1 ex. 14 | BRAF | pTERT | ATRX | NTRK1 |
|---|---|---|---|---|---|---|---|---|---|---|---|---|---|---|---|
| 1 | M | Primary | 30 | Lateral ventricle | A2 | WT | WT | G34R + R26H | WT | WT | WT | WT | WT | LOSS | 38% |
| 2A | M | Primary | 43 | Lateral ventricle | A2 | R132G | WT | WT | WT | WT | WT | WT | WT | LOSS | 29% |
| 2B | M | Recurrence | 47 | Lateral ventricle | A2 | R132G | WT | WT | WT | WT | WT | WT | WT | LOSS | 20% |
| 3 | F | Primary | 69 | Thalamus | GBM | WT | WT | WT | WT | WT | WT | WT | C250T | LOSS | 25% |
| 4 | M | Primary | 16 | Brainstem | GBM | WT | WT | K27M | WT | WT | WT | WT | WT | RETAINED | 29% |
| 5 | M | Primary | 68 | Corpus callosum | GBM | WT | WT | WT | WT | WT | WT | WT | C228T | RETAINED | 34% |
| 6 | F | Primary | 31 | Spinal cord | GBM | WT | WT | K27M | WT | WT | WT | WT | WT | RETAINED | 17% |

**Table 4.** Molecular profiling and protein expression of the 6 NTRK1 translocated cases.

The comparison between NTRK1 positive and negative cases are reported in Table 5.

| | NTRK1 translocation | | |
|---|---|---|---|
| | **Negative** | **Positive** | **P-value** |
| **N** | 35 | 6 | NA |
| **Sex ratio (M/F)** | 1.69 (22/13) | 0.5 (2/4) | 1.000 |
| **Age at surgery in years, median (range)** | 47 (17 – 81) | 43 (16 – 69) | 1.000 |
| **Location, % (n)** | | | 0.218 |
| - **Non-thalamic diencephalic** | 57 (20/35) | 50 (3/6) | |
| - **Thalamic** | 9 (3/35) | 17 (1/6) | |
| - **Brainstem** | 0 | 17 (1/6) | |
| - **Cerebellar** | 14 (5/35) | 0 | |
| - **Spinal cord** | 20 (7/35) | 17 (1/6) | |
| **Diagnosis, % (n)** | 46 (16/35) A2-3<br>6 (2/35) OD3<br>48 (17/35) GBM | 33 (2/6) A2<br>66 (4/6) GBM | 0.640 |
| **Median OS in months** | 50.4 months | 18.7 months | 0.095 |
| **IDH mutation, % (n)** | 3 (1/35) | 17 (1/6) | |
| **ATRX loss, % (n)** | 14 (5/35) | 50 (3/6) | 0.268 |
| **pTERT mutation, % (n)** | 34 (12/35) | 33 (2/6) | 1.000 |
| **C228T (n):** | 6 | 1 | |
| **C250T (n):** | 6 | 1 | |
| **H3F3A-K27M mutation, % (n)** | 20 (7/35) | 33 (2/6) | 0.607 |
| **FGFR1 mutation, % (n)** | 9 (3/35) | 0 | 1.000 |
| **BRAF mutation, % (n)** | 3 (1/35) | 0 | 1.000 |

**Table 5.** Clinical, histological and molecular characteristics in patients with NTRK1 translocated versus NTRK1 not-translocated MLG

The Fisher exact test did not find any correlation among NTRK1 gene rearrangements and clinical-pathological data (age, gender, tumour localization) and other molecular markers (IDH1/2, H3F3A, HIST1H3B, FGFR1, pTERT, BRAF and ATRX).

The Kaplan Meier survival curve showed a tendency to a worse prognosis in patients with translocation of NTRK1 even if the significance threshold is not reached (p-value 0.095, Figure 10).

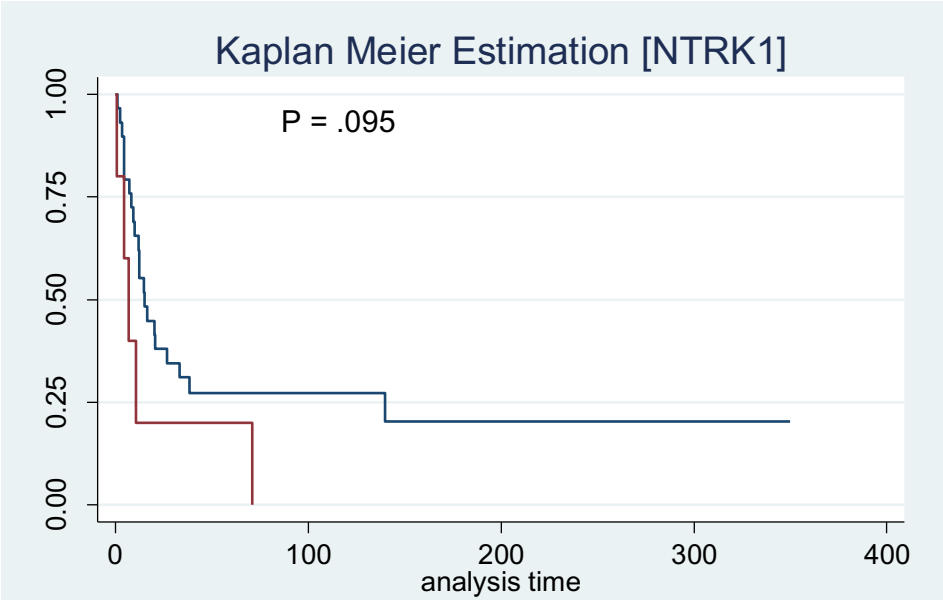


**Figure 10.** Kaplan Meier curve. In red, the survival curve of translocated patients

In the following pages, some images of FISH analysis of positive cases are showed.

*Case number 1* (Figure 11A and B) showed a translocation of NTRK1 in 38% of cells in 7 high powered fields for a total number of 100 cells.

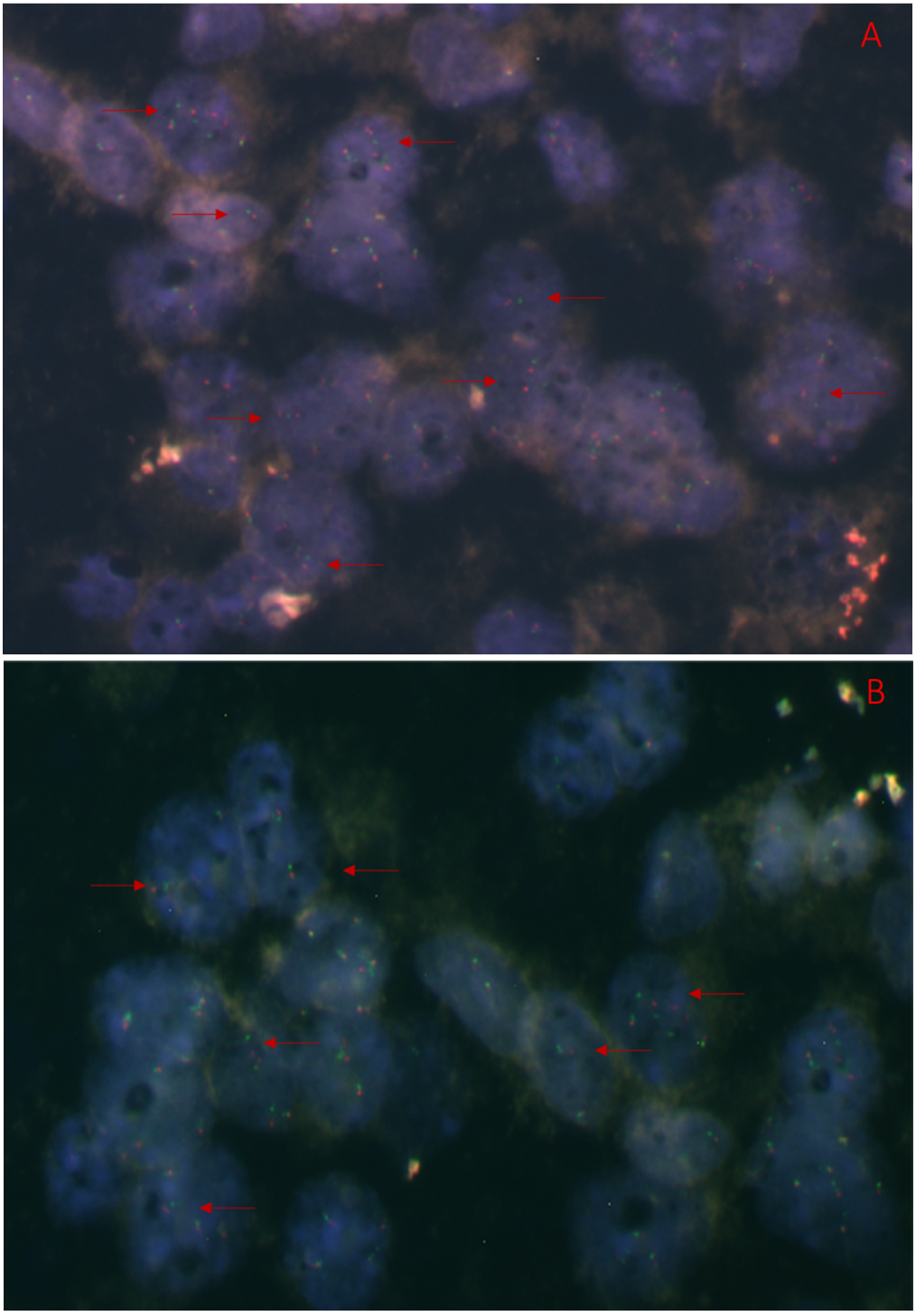


**Figure 11 A-B.** The red arrows in the images indicate the NTRK1 gene rearrangement in case number 1. Real magnification: 630X.

*Case number 2:* primary (case 2A) (Figure 12A and B) and recurrent (case 2B) (Figure 13A and B) tumours demonstrated a concordance in NTRK1 results, showing both a translocation in respectively 29% and 20% of cells.

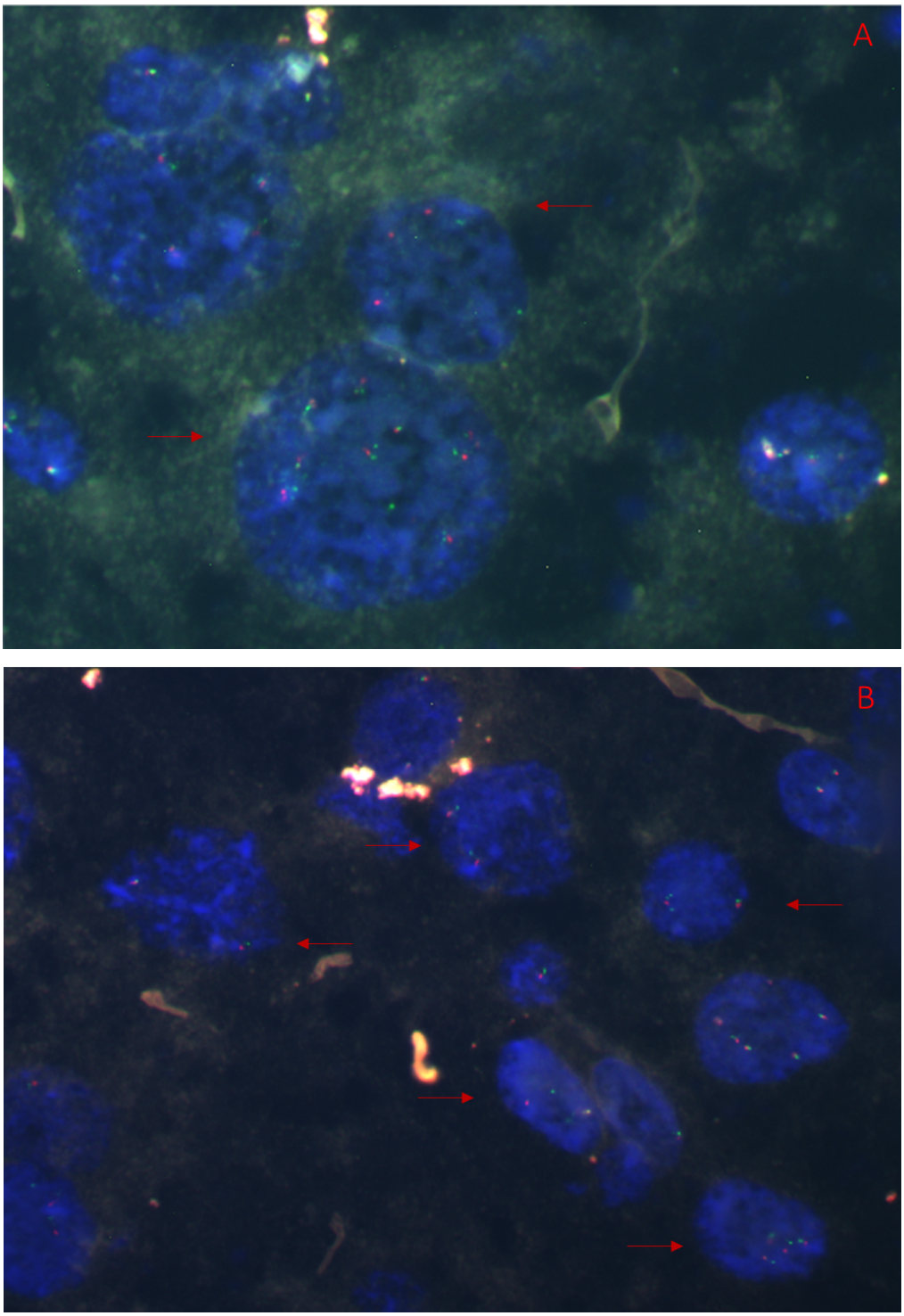


**Figure 12 A-B.** The red arrows in the images show the NTRK1 gene rearrangement in case number 2A, the primary tumour. Real magnification: 1000X.

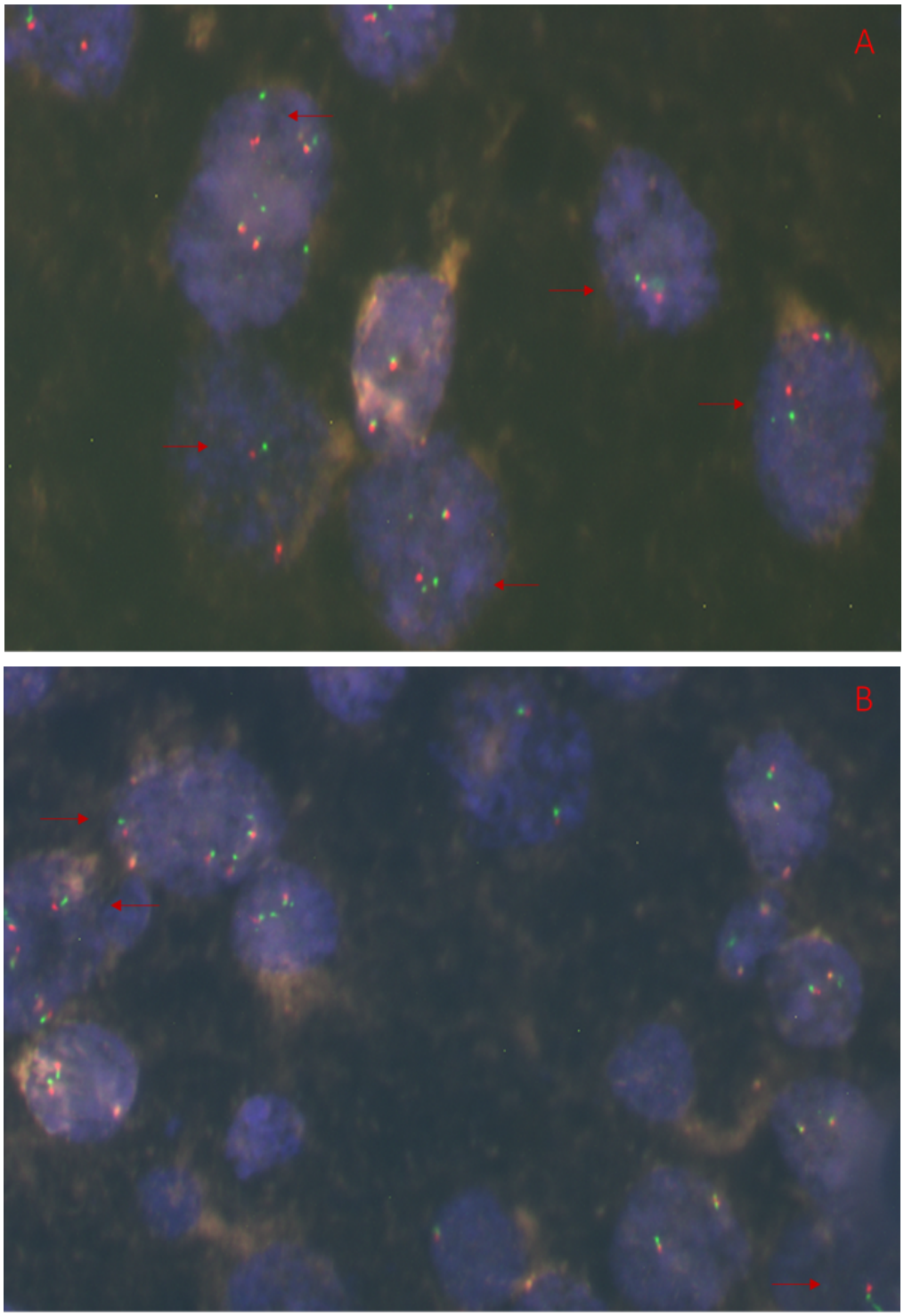


**Figure 13 A-B.** The red arrows in the images show the NTRK1 gene rearrangement in case the recurrent tumour (case 2B). Real magnification: 1000X.

*Case number 3* (Figure 13 A-B) reported a gene rearrangement in 25% of cells.

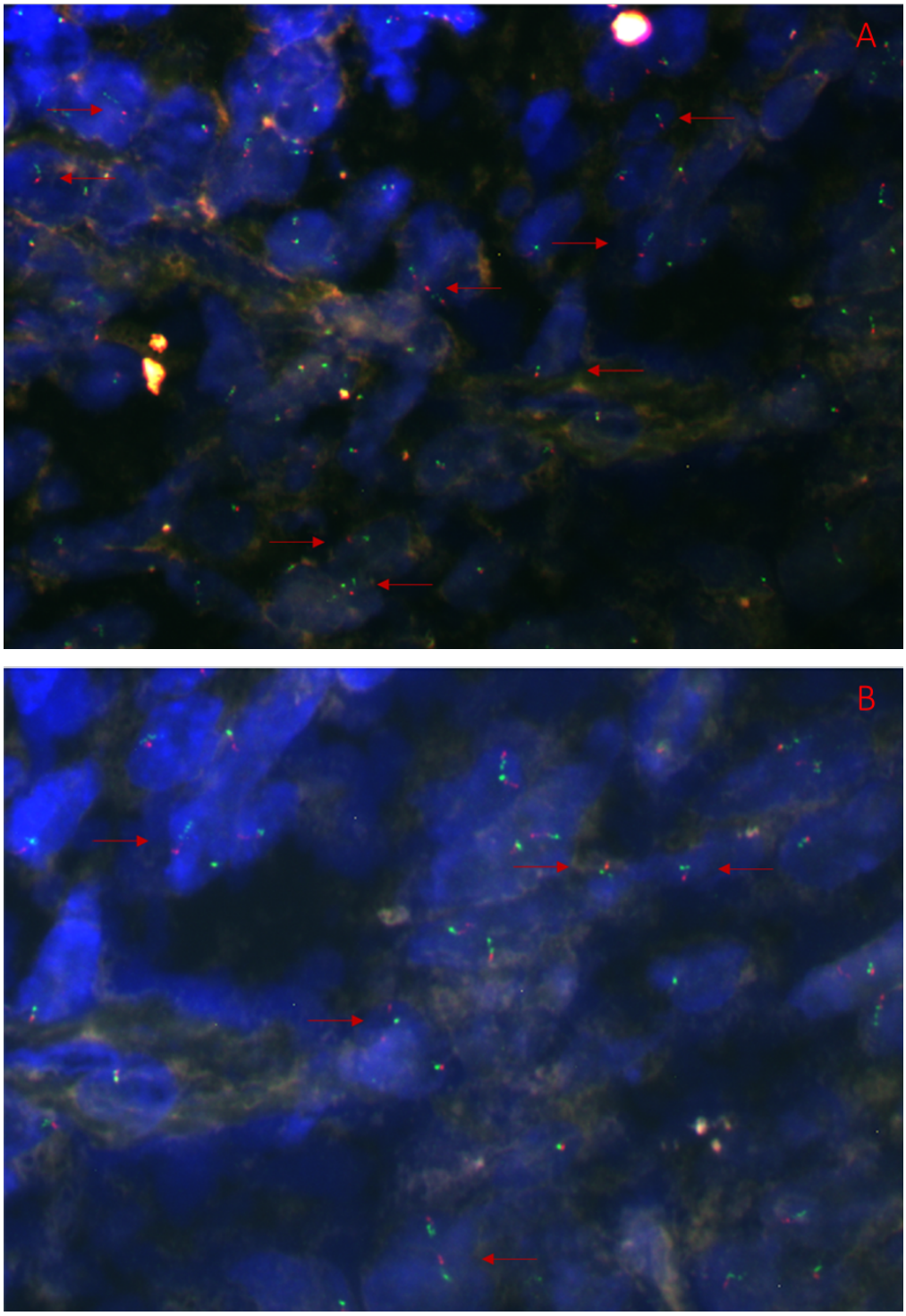


**Figure 13 A-B.** The red arrows in the images indicate the NTRK1 gene rearrangement in case number 3. Real magnification: 630X.

*Case number 4* shows 29% of cells translocated for NTRK1 (Figure 14A and B).

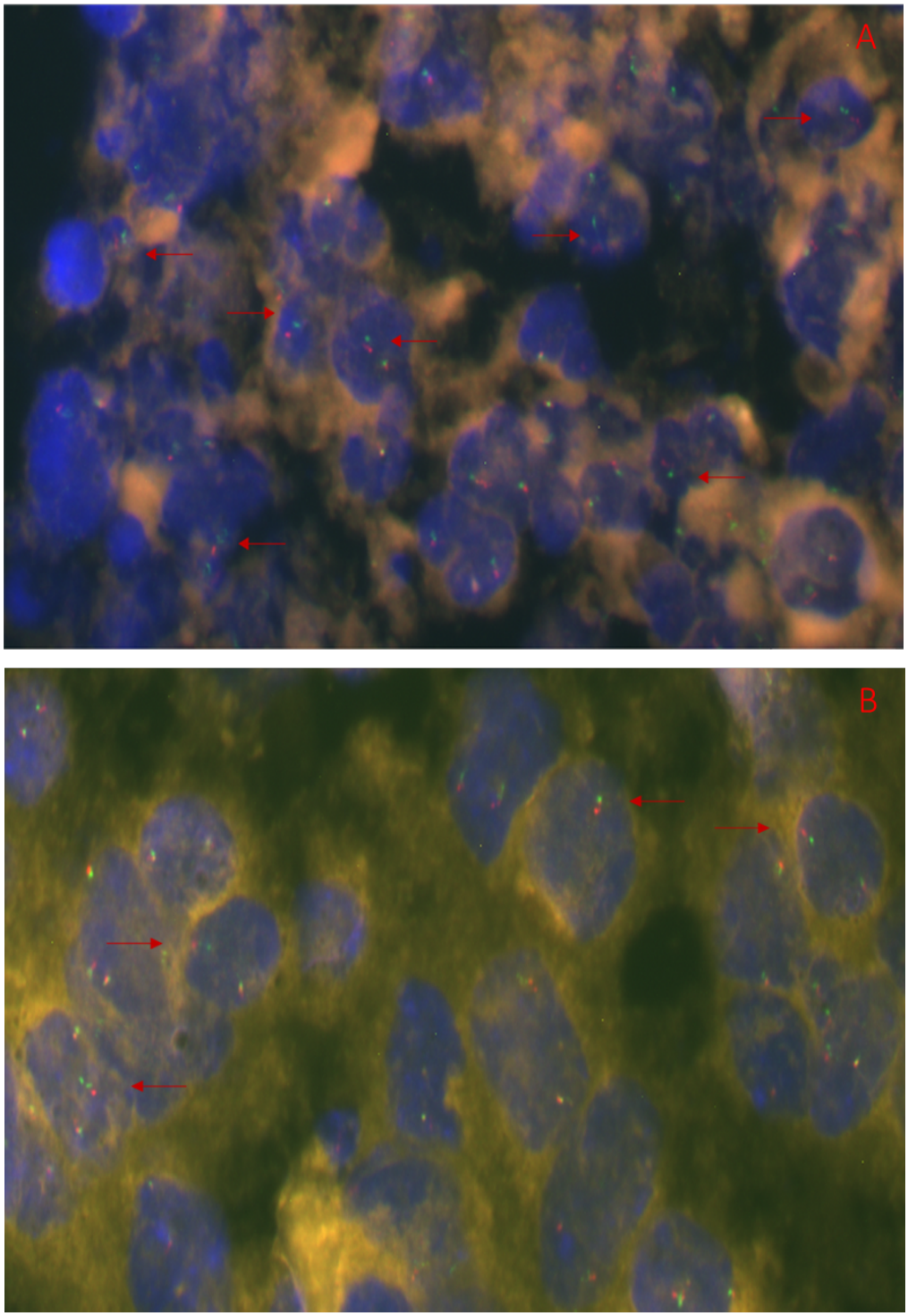


**Figure 14 A-B.** The red arrows in the images show the NTRK1 gene rearrangement in case number 4. Real magnification: 630X.

*Case number 5* reported NTRK1 translocation (figure 15A and B) in 34% of cells.

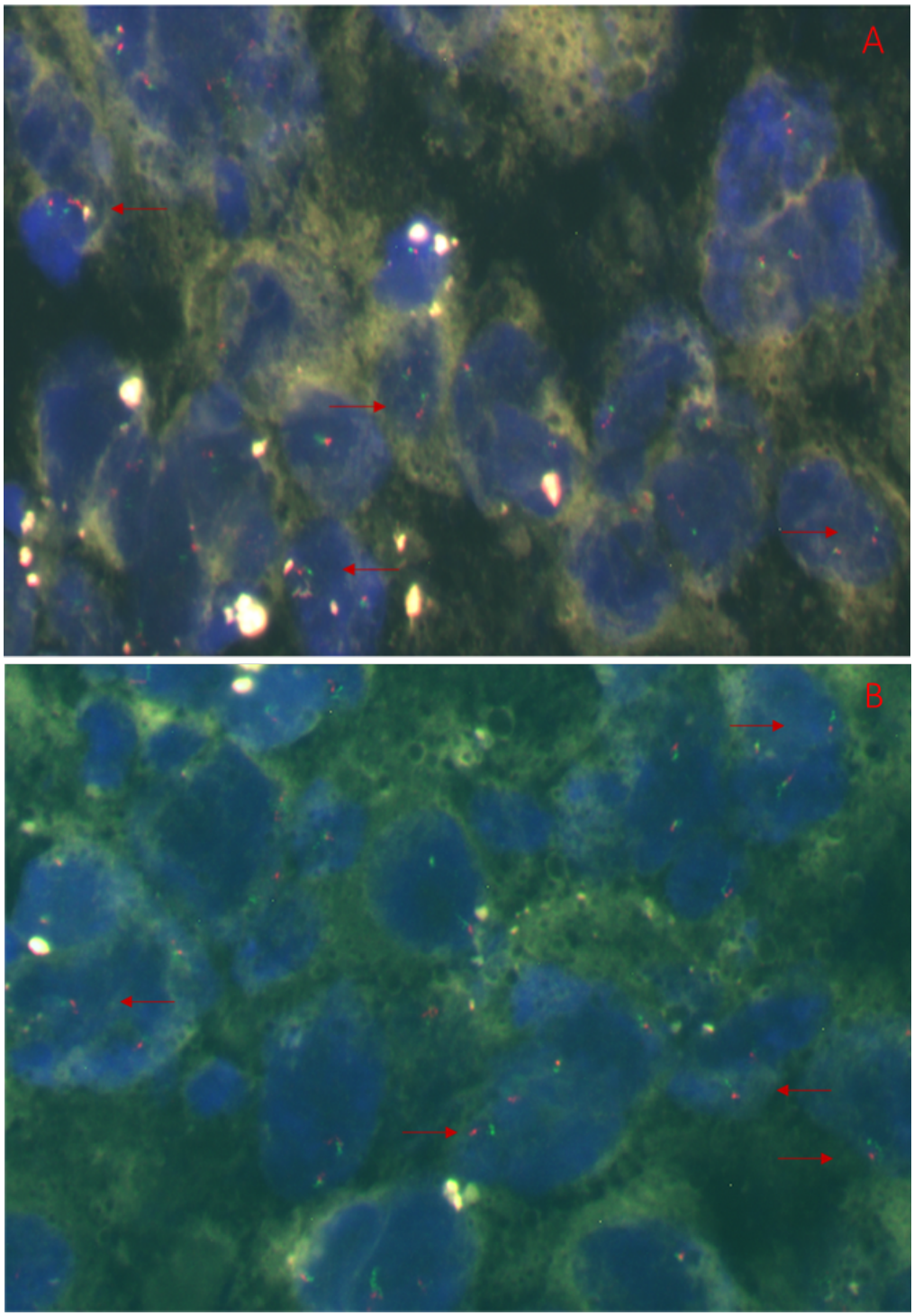


**Figure 15 A-B.** The red arrows in the images write down the NTRK1 gene rearrangement in case number 5. Real magnification: 630X.

*Case number 6* (Figure 16A and B) displays the gene rearrangement in 17% of cells.

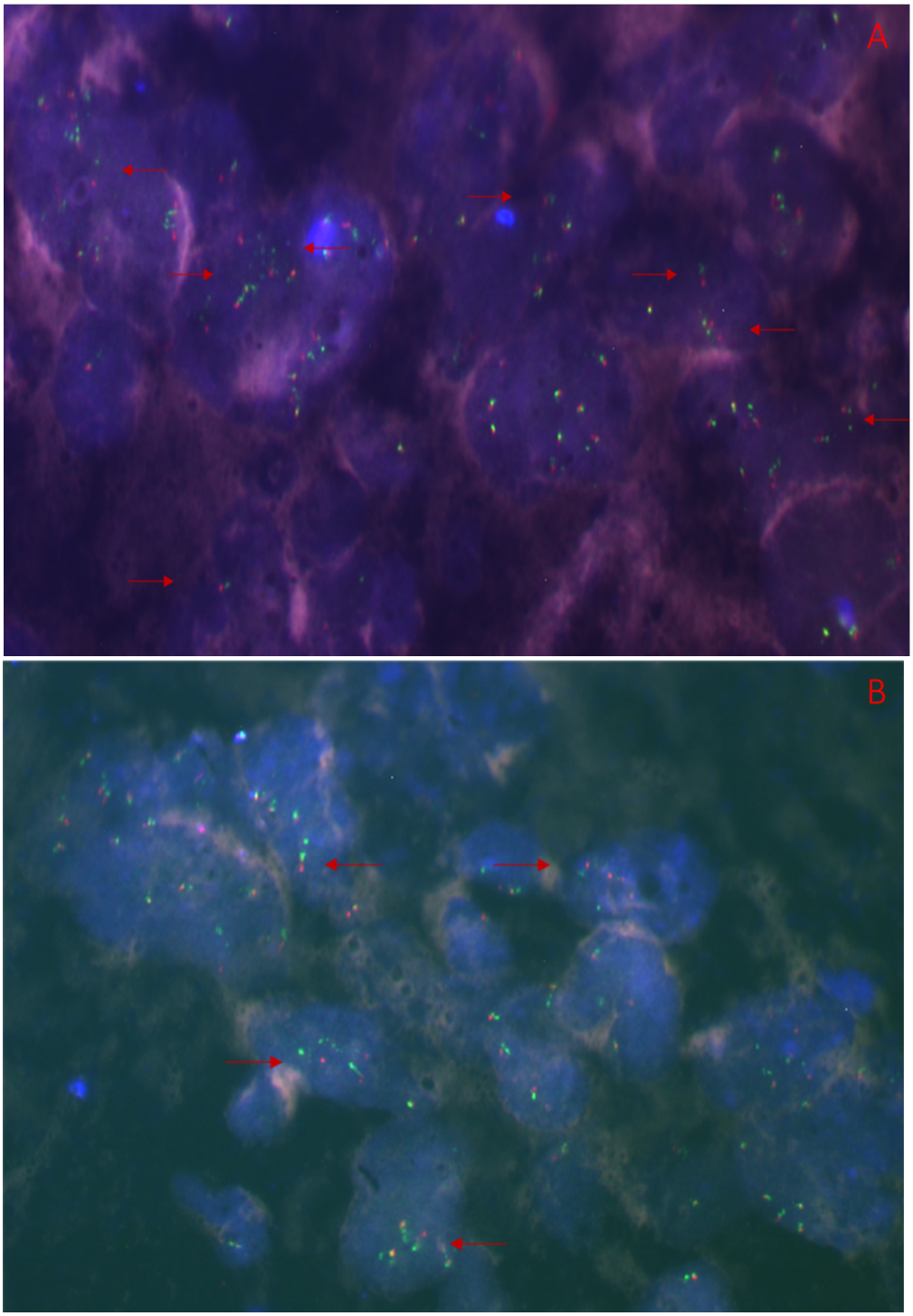


**Figure 16 A-B.** The red arrows in the images show the NTRK1 gene rearrangement in case number 6. Real magnification: 630X.

The other 35 (85%) cases did not show any translocation involving NTRK1 gene.

### 4.1.2 NTRK2 and NTRK3 status

Regarding NTRK2 gene we were able to obtain results of 43 (95.5%) cases out of 45. Whereas, for NTRK3 gene we reached a result in 42 (93.3%) out of 45 specimens, due to the lack of tissue sample.

Nevertheless, none of the cases reported NTRK2 or NTRK3 gene rearrangements.

## 4.3 Molecular analysis in circumscribed gliomas[76]

### 4.3.1 Clinico-pathological features of pilocytic astrocytomas, gangliogliomas, ependymomas and DNET

We retrospectively identified 108 pilocytic astrocytomas, 80 were from GH Pitié-Salpêtrière and 28 from AOU Maggiore della Carità. We analysed both the primary and the recurrent tumour of 4 patients (posterior fossa (2), supratentorial (1) and optic pathway (1)).

We retrospectively identified 75 grade II and 7 grade III gangliogliomas (all GH Pitié-Salpêtrière), 100 grade II (81 GH Pitié-Salpêtrière, 19 AOU Maggiore della Carità) and 26 grade III ependymomas (21 GH Pitié-Salpêtrière, 5 AOU Maggiore della Carità) and 7 DNETs (all GH Pitié-Salpêtrière).

The location of the tumours and the main demographic and pathological features are reported in Table 6.

| | PA | GG II | GG III | EP II | EP III | DNET |
|---|---|---|---|---|---|---|
| **N** | **108** | **75** | **7** | **100** | **26** | **7** |
| **Sex (M/F)** | 60/48 | 39/36 | 2/5 | 52/48 | 14/12 | 3/4 |
| **Mean age at surgery in years ± SD, (range)** | 34 ± 15 (16 – 76) | 34 ± 14 (15 - 69) | 44 ± 18 (20 - 65) | 45 ± 16 (16 – 81) | 40 ± 19 (16 – 76) | 28 ± 12 (15 – 48) |
| **Location, % (n)** | | | | | | |
| **Supratentorial** | 28.7 (31/108) | 56 (42/75) | 42.8 (3/7) | 11 (11/100) | 53.9 (14/26) | 28.6 (2/7) |
| **Posterior Fossa** | 47.2 (51/108) | 12 (9/75) | 42.8 (3/7) | 25 (25/100) | 26.9 (7/26) | 0 |
| **Optic pathway** | 8.3 (9/108) | 0 | 0 | 0 | 0 | 0 |
| **Spinal cord** | 3.7 (4/108) | 1.3 (1/75) | 0 | 39 (39/100) | 19.2 (5/26) | 0 |
| **Not available** | 12.1 (13/108) | 30.7 (23/75) | 14.4 (1/7) | 25 (25/100) | 0 | 71.4 (5/7) |

**Table 6.** Characteristics of the cohort (SD: standard deviation, PA: pilocytic astrocytoma, GG: ganglioglioma, EP: ependymoma, DNET: dysembryoplastic neuroepithelial tumour)

### 4.3.2 FGFR1 activating mutations in circumscribed gliomas

Activating FGFR1 mutations were identified in 15/108 (13.9%) pilocytic astrocytomas: p.Asn546Lys (8 cases), p.Asn546Asp (1 case) and p.Lys656Glu (6 cases) (Table 7). In one patient, the p.Asn546Lys mutation was present at progression in the recurrent tumour. Strikingly, mutations were more frequent in optic pathway compared to other locations (6/9 vs 9/108; $p=4.10^{-5}$).

No statistically significant different distribution of sexes (p=0.26) and age (p=0.56) were observed between mutated and wild-type pilocytic astrocytomas.

FGFR1 was mutated in 3/75 grade II vs 2/7 grade III gangliogliomas (p=0.05), 1/7 DNET, 1/100 ependymoma grade II (Table 8).

| Location | p.Asn546Lys | p.Asn546Asp | p.Lys656Glu | *wild-type* | mut/total (%) |
|---|---|---|---|---|---|
| Supratentorial | 2* | 0 | 3 | 26 | 5/31 (16.1 %) |
| Posterior Fossa | 2 | 0 | 1 | 48 | 3/51 (5.9 %) |
| Optic pathway | 3 | 1 | 2 | 3 | 6/9 (66.7 %) |
| Spinal cord | 0 | 0 | 0 | 4 | 0/4 (0.0 %) |
| Not available | 1 | 0 | 0 | 12 | 1/13 (6.3%) |

*corresponding to the primitive and recurrent tumour of the same patient

**Table 7.** FGFR1 mutations' distribution in pilocytic astrocytoma

| | FGFR1 mutations | | | | BRAF mutation |
|---|---|---|---|---|---|
| | p.Asn546Lys | p.Asn546Asp | p.Lys656Glu | p.Lys656Asn | p.Val600Glu |
| GG grade II | 1/75 (1.3%) | 0 | 2/75 (2.6%) | 0 | 14/75 (18.7%) |
| GG grade III | 2/7 (28.6%) | 0 | 0 | 0 | 0 |
| EP grade II | 1/100 (1%) | 0 | 0 | 0 | 0 |
| EP grade III | 0 | 0 | 0 | 0 | 0 |
| DNET | 0 | 0 | 0 | 1/7 (14.3%) | 0 |

GG: ganglioglioma, EP: ependymoma, DNET: dysembryoplastic neuroepithelial tumour

**Table 8.** BRAF and FGFR1 mutations' distribution in other circumscribed gliomas

### 4.3.3 BRAF mutation analysis

We found 3/108 (2.8%) pilocytic astrocytomas with p.Val600Glu mutation, 6/108 (5.6%) with p.Thr599_Val600insThr mutation (4/6 cases with c.1797_1798insACA, 2/6 with c.1796_1797insTAC), 1/108 case with p.Val600_Lys601>Glu (c.1799_1801delTGA) (Table 9). In Figure 17A-B-C are reported the electropherograms of insertions and deletion detected in BRAF exon 15.

The p.Val600Glu mutation was found in 14/75 (18.2%) grade II gangliogliomas. The p.Val600Glu mutation seems to be associated to a younger age (23 Vs 36 years, p=0.0058) but did not show any different distribution between sexes (p=0.88).

None of ependymomas grade II and III were BRAF mutated (Table 8).

In this population we found no p.Thr599_Val600insThr mutation, in contrast to pilocytic astrocytomas (6/108 vs 0/215, p=2.10-3) and no p.Val600_Lys601>Glu.

| **Location** | **p.Val600Glu** | **p.Thr599_ Val600insThr** | **p.Val600_ Lys601>Glu** | ***wild-type*** | **mut/total (%)** |
|---|---|---|---|---|---|
| Supratentorial | 2 | 2* | 0 | 27 | 4/31 (12.9%) |
| Posterior Fossa | 0 | 3 (2* + 1**) | 0 | 48 | 3/51 (5.9%) |
| Optic pathway | 0 | 0 | 0 | 9 | 0/9 (0%) |
| Spinal cord | 0 | 0 | 0 | 4 | 0/4 (0%) |
| Not available | 1 | 1** | 1 | 10 | 3/13 (23%) |

* c.1797_1798insACA - ** c.1796_1797insTAC

Table 9. BRAF mutations' distribution in pilocytic astrocytomas

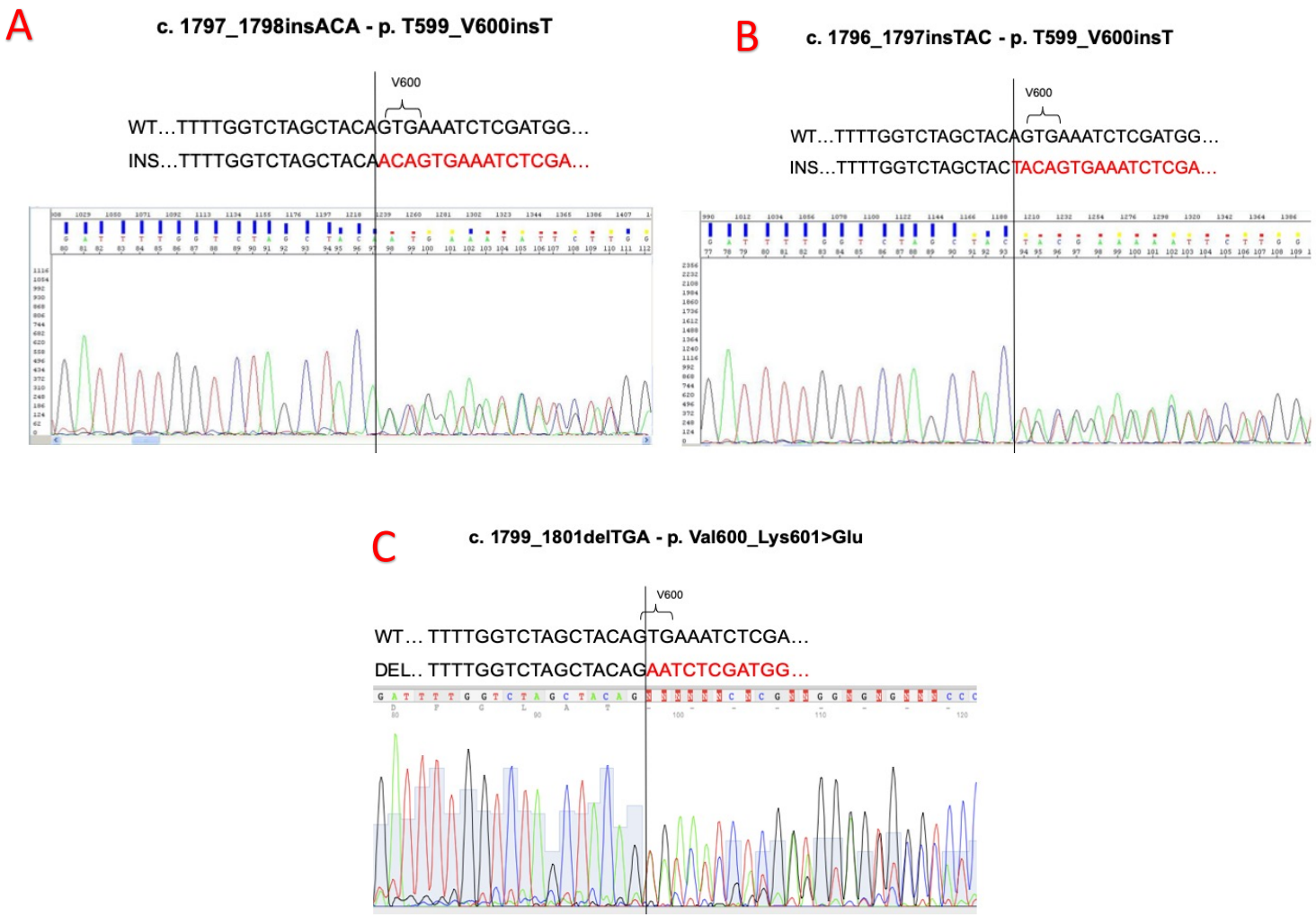


Figure 17A-B-C. Electropherograms of BRAF insertions

# 5. DISCUSSION

Gliomas are the most common primary tumours of the central nervous system representing 81% of malignant CNS tumours[77]. According to 2016 World Health Organization classification, a specific subgroup of diffuse gliomas arise from midline structures which include ventricles, cerebellum, optic pathway/chiasmatic region, corpus callosum, hippocampus, hypothalamus, thalamus, pineal gland, brainstem, and spinal cord. This subgroup is typically defined by the presence of H3K27M mutation, occurring mainly in paediatric age and characterized by a poor prognosis, independently to the histological grading but also present in the adult population. Moreover, the prognostic impact of H3K27M mutation in adult MLGs differs from paediatric gliomas, showing no significant differences with H3K27-WT gliomas[78]. This suggests alternative pathogenic mechanisms between the two groups of MLGs. However, the presence of tumours in midline structures is generally associated with a poor prognosis also due to technical difficulties for surgical complete resection[79]. The current therapeutical approach for paediatric and adult diffuse gliomas is surgery associated with radio and/or chemotherapy, depending on the grade and differentiation of the tumour[80], but in MLGs since the surgical resection is incomplete in most cases, alternative therapeutic strategies are encouraged[34,63].

This retrospective study shows that adult MLG constitute a heterogeneous group with mostly high-grade neoplasms and clinical and histomolecular characteristics differing from both pediatric MLG and adult supratentorial high-grade gliomas. We identified two main subgroups based on the presence of histone H3 or IDH1 mutations, and identified hotspot FGFR1 mutations and NTRK1 rearrangements as potential therapeutic targets in this population.

The most prominent molecular subgroup consisted of histone H3 mutant MLG, in line with previous studies showing a strong association between histone H3 mutations and gliomagenesis of midline tumours[2,3,6,9,81]. However, we observed a lower prevalence of histone H3 mutations compared to pediatric high-grade thalamic and brainstem gliomas (70-80%). In addition, clinical and molecular characteristics of patients from our cohort with histone H3 mutant MLG differed from pediatric patients. Firstly, despite histone H3 mutations were associated with younger age at diagnosis in the

French cohort (median 33 years vs. 53 years, p=6*10-5), we found H3 mutation in patients over 60 years, indicating that screening for histone H3 mutants should be considered in all MLG, regardless of age. Moreover, in contrast to pediatric gliomas, we found that histone H3 mutations were not associated with a worse prognosis compared to the other IDH wild-type gliomas[14].

The other main driver alteration is IDH mutation, which in the French cohort occurs specifically in brainstem (6/24 vs. 0/78 in other midline localizations). The majority of IDH1 mutations in this cohort were non-R132H, indicating that the widely used anti-R132H immunohistochemistry staining is not appropriate in brainstem gliomas and have probably underestimated the proportion of IDH1-mutant tumours[25]. Systematic IDH1 sequencing should be performed whenever feasible in brainstem gliomas. Also in the Italian cohort we found a rare IDH1 mutation (R132G) among only 4/46 mutated cases. Indeed, as observed in hemispheric gliomas, IDH1 mutation is associated with better outcome (median survival [MS] = 54.1 versus 15.9 months in French cohort), and may in part explain why adults with brainstem gliomas have a better survival than children[21,25,82]. In addition to its prognostic value, the recognition of IDH1 mutations may open therapeutic opportunities, as inhibitor of IDH1-mutant enzymes have demonstrated antitumour potential and entered clinical trials for patients with IDH1-mutations[23,83,84].

In addition to IDH1 mutation, we identified here other potentially targetable hotspot mutations affecting N546 and K656 residues of FGFR1 in 18% of cases in the French cohort and 7% of Italian cohort. FGFR1 mutations were not associated with any specific location or any molecular subgroup. Somatic FGFR1 N546 and K656 mutations were previously reported in several other cancer types[85], comprising a wide range of central nervous system (CNS) tumours, including rosette-forming glioneuronal tumours[86,87], dysembryoplastic neuroepithelial tumours[88], pilocytic astrocytomas[44,89,90], diffuse leptomeningeal tumour with glial and neuronal markers[91], pediatric thalamic gliomas[21,22,92]. These studies analysed isolated cases or small cohorts, which made difficult the assessment of the incidence of FGFR1 mutations in this population. FGFR1 N546 and K656 mutants lead to constitutive activation of FGFR1 tyrosine kinase and downstream RAS-MAPK signalling, contributing to transformation[93-95], and can be targeted by a number of oral inhibitors: notably, the

recent clinical development[96] of a novel irreversible FGFR inhibitor (e.g. TAS-120) that demonstrated potent activity against N550K mutants[24,97] open new therapeutic opportunities in this population. In our study, we demonstrated that FGFR1 mutations are restricted to midline structures because absent in a huge cohort of hemispheric gliomas and absent also in public repositories (i.e. Cosmic); these mutations may be considered as a hallmark of midline gliomas.

BRAF V600E is another actionable target, which has been rarely associated with H3K27M in pediatric gangliogliomas and diffuse midline gliomas[7,98-100]. However, the French cohort did not show any V600 BRAF mutation in all the 68 sequenced patients while in the Italian cohort we found 1 V600E mutated case.

Our study was restricted by the scarcity of available tumour material limiting both histopathological and genomic analyses. Therefore, our genomic analyses were restricted to a panel of selected molecular alterations, while several samples were exhausted at the time of this retrospective analysis. However, the majority of the patients could be assessed for TERT promoter status. As observed in adult supratentorial glioblastomas, TERTp mutation, which affected 37% of French cases and 35% of Italian cases, was associated with older age, grade IV, poor survival, (also with EGFR amplifications and loss of chromosome 10 and deletion of CDKN2A as reported in the French cohort). Survival of these patients was particularly poor (OS = 9.1 months vs. 24.2 months for patients without TERTp mutations in the French cohort and 10.5 months vs. 64.2 months in the Italian cohort), even compared to adult patients with hemispheric glioblastomas followed in French institution (OS = 13.5 months)[83] which may be related to the inability to resect these tumours. TERT promoter appears therefore a biomarker of poor survival in patients with adult MLG.

In this study, we chose to investigate for rearrangements in NTRK family genes since new targeted therapies are available in clinical trials and show encouraging results in many tumours harbouring these genetic lesions. NTRKs in normal condition encode Trk, a tyrosine kinase receptor, and when activated by the binding of their ligands NGF promotes signal transduction involved in proliferation and cell survival[61]. Rearrangements of NTRKs are associated to constitutive activation of Trk that is an important driver in tumour development in many human tumours like, colorectal, lung and GBMs[101].

The results of our study indicated a relative high frequency (15%) of NTRK1 rearrangements, that were randomly distributed in our MLG cohort (Italian), independently to the histological grading. Our data are poorly comparable with literature, since few authors have evaluated NTRKs rearrangements in adult gliomas and, mainly in GBMs reporting a low percentage (1-2.5%) of translocations[102].

Regarding MLGs, there are few studies that have reported NTRKs rearrangements in pilocytic astrocytomas and DIPGs in childhood with variables frequencies ranging from 1% to 4%[44,103].

The main result of our study consisted in demonstrating that NTRK1 rearrangements are not sporadic event in this kind of tumours but show a relatively high frequency. Since the new therapeutical strategies in several types of solid tumours are addressed to the inhibition of specific tyrosin kinase activated receptors, the demonstration of the presence of this kind of rearrangements opens the possibility of a new targeted therapy also in MLGs. Moreover, our data showed a tendency of worse prognosis in cases harbouring NTRK1 rearrangements, even if statistical significance was not reached.

FISH analysis although easy to perform also in routine samples, is not able to identify a specific gene partner of fusion and, moreover, is not informative of the function of the new chimeric protein. For this reason, FISH can be used as a screening technique, but the positive cases need to be additionally evaluated by Next Generation Sequencing, in order identify the real function of chimeric protein.

Since the prognosis of MLGs is unchanged in last decades and therapeutical approaches are limited to standard cares, there is an urgent need to explore new targetable biomarkers.

Up to now, the encouraging results seem to come from the discovering that the inhibition of TRK-like NTRK1 in MLGs can improve the prognosis and it can be a valid alterative for conventional therapeutical strategy. Taken together with FGFR1 mutations, our results seem to confirm that they can constitute a promising field of translational research.

MAPK/ERK pathway is involved in the pathogenesis of pilocytic astrocytoma and other circumscribed gliomas. In this study we reported the frequency of FGFR1 and BRAF activating mutations in a series of 323 adult circumscribed gliomas.

FGFR1 mutations have been already described in pilocytic astrocytomas[44,89,90,104,105]. Here we found an unexpected high frequency of FGFR1 mutation in optic-pathway pilocytic astrocytomas of adults (6/9; $p=4.10^{-5}$) not affected by Neurofibromatosis type-1 (NF1). To the best of our knowledge, this is the first description of the association between FGFR1 activating mutations and optic pathway gliomas. This finding may be related to the role of FGFR1 signalling in midline commissure development[106] and the anterior part of the brain[107]. Interestingly, in diffuse gliomas FGFR1 mutations are restricted to midline tumours, as reported in our study[75]. This finding has important practical consequences: as optic pathway PA are hardly accessible to surgery, they could be excellent candidates to anti-FGFR therapies. Our data suggest that FGFR1 activating mutation may be associated with tumour progression in PA as it has been acquired during the transformation of the tumour in one patient, and also in gangliogliomas as it is found in 2/7 grade III vs 3/75 grade II (p=0.05).

As expected, we found nearly 20% of BRAF mutation (p.Val600Glu) in ganglioglioma independently of the tumour grading.

In PA, in addition to the p.Val600Glu, we found other BRAF activating mutations. The threonine insertion (p.Thr599_Val600insThr) causes an increased kinase activity and cellular MEK/ERK activation comparable to those of p.Val600Glu mutation[108]. Strikingly, p.Thr599_Val600insThr mutation was even more frequent than p.Val600Glu mutation (6/108 (5.6%) vs 3/108 (2.8%) in PA, while it was absent in the other circumscribed gliomas (GG, EP, DNET). The p.Thr599_Val600insThr can be caused by two different nucleotide changes: c.1797_1798insACA has never been reported before in pilocytic astrocytoma, but only in pleomorphic xanthoastrocytomas[55], whereas the c.1796_1797insTAC has been reported in pilocytic astrocytomas[108,109]. We also found a three-base pair deletion (c.1799_1801delTGA) leading to the substitution of Val600 and Lys601 by a Glu600, which has been reported mostly in papillary thyroid carcinomas[110], but not in central nervous systems tumours

(https://cancer.sanger.ac.uk/cosmic/mutation/overview?id=1133). This deletion results in dramatic increase of BRAF kinase activity and increased tumourigenicity[109]. While the BRAF p.Val600Glu mutated tumours are sensitive to anti-BRAF, this is unknown for the other BRAF mutations which can be targeted by an anti-MEK, inhibiting the downstream effectors. However, taken together these findings provide strong opportunities for precision therapies mainly for tumour not easily accessible to surgery.

In conclusion, our findings reinforce the need for histological confirmation and molecular analyses in adult patients with MLG, given the significant heterogeneity among midline tumours and the presence of recurrent potentially targetable molecular alterations in these fatal diseases. While IDH1 and TERT promoter mutations may assist treatment stratification in adult patients with MLG, we show here that histone H3 mutations do not confer worse prognosis in adult patients with MLG. Our finding of frequent and potentially targetable FGFR1 mutations and NTRK translocation have important clinical implications in the current context of targeted therapies, and further reinforces the need for molecular analyses.
Moreover, even if circumscribed gliomas may not generally represent an aggressive or life-threatening disease, in some cases a therapeutical alternative to surgery may be the only chance for treatment, especially when the tumour belongs to deep brain structures, such as optic pathway. For this reason, molecular analysis of the mutational hotspots discussed in this study could be part of the routine procedures.

# 6. FUTURE PERSPECTIVES

We will confirm the presence of NTRK1 rearrangements in FISH-positive MLG also for the characterization of the fusion by next generation sequencing (NGS) technique.

We will extend the NTRK analysis in adult circumscribed gliomas to assess the presence and distribution of gene rearrangements.

We would also expand the cohort of both MLG and circumscribed gliomas in order to confirm our data and we would also extend the genetic analysis in other genes involved in the MAPK pathway by using NGS gene panels.

# REFERENCES


1- Kleinschmidt-DeMasters BK and Mulcahy LJM. (2018) H3 K27M-mutant gliomas in adults vs. children share similar histological features and adverse prognosis. Clinical Neuropathology 2:53-63. doi: 10.5414/NP301085.

2- Castel D, et al. (2015) Histone H3F3A and HIST1H3B K27M mutations define two subgroups of diffuse intrinsic pontine gliomas with different prognosis and phenotypes. Acta Neuropathol (Berl) 130:815–827. doi: 10.1007/s00401-015-1478-0.

3- Wu G, et al. (2012) Somatic histone H3 alterations in pediatric diffuse intrinsic pontine gliomas and non-brainstem glioblastomas. Nat Genet 44:251–253. doi: 10.1038/ng.1102

4- Buczkowicz P, et al. (2014) Histopathological spectrum of paediatric diffuse intrinsic pontine glioma: diagnostic and therapeutic implications. Acta Neuropathol (Berl) 128:573–581. doi: 10.1007/s00401-014-1319-6

5- Gielen GH, et al. (2013) H3F3A K27M mutation in pediatric CNS tumours: a marker for diffuse high-grade astrocytomas. Am J Clin Pathol 139:345–349. doi: 10.1309/AJCPABOHBC33FVMO

6- Khuong-Quang D-A, et al. (2012) K27M mutation in histone H3. 3 defines clinically and biologically distinct subgroups of pediatric diffuse intrinsic pontine gliomas. Acta Neuropathol (Berl) 124:439–447. doi: 10.1007/s00401-012-0998-0

7- Solomon DA, et al. (2016) Diffuse Midline Gliomas with Histone H3-K27M Mutation: A Series of 47 Cases Assessing the Spectrum of Morphologic Variation and Associated Genetic Alterations. Brain Pathol 26(5):569-80. doi: 10.1111/bpa.12336.

8- Sturm D, et al. (2012) Hotspot mutations in H3F3A and IDH1 define distinct epigenetic and biological subgroups of glioblastoma. Cancer Cell 22:425–437. doi: 10.1016/j.ccr.2012.08.024

9- Taylor KR, et al. (2014) Recurrent activating ACVR1 mutations in diffuse intrinsic pontine glioma. Nat Genet 46:457–461. doi: 10.1038/ng.2925

10- Korshunov A, et al. (2016) Histologically distinct neuroepithelial tumours with histone 3 G34 mutation are molecularly similar and comprise a single nosologic entity. Acta Neuropathol (Berl) 131:137–146. doi: 10.1007/s00401-015-1493-1

11- Bjerke L, et al. (2013) Histone H3.3. mutations drive pediatric glioblastoma through upregulation of MYCN. Cancer Discov 3:512–519. doi: 10.1158/2159-8290.CD-12-0426

12- Louis DN et al., (2016) WHO Classification of Tumours of the Central Nervous System, WHO Classification of Tumours, Revised 4th Edition, Volume 1. IARC publications. ISBN-13 9789283244929

13- Lulla RR, Muhs Saratsis A, and Hashizume R. (2016) Mutations in Chromatin Machinery and Pediatric High-Grade Glioma. Science Advances 2(3): e1501354. doi: 10.1126/sciadv.1501354

14- Meyronet D, et al. (2017) Characteristics of H3 K27M-mutant gliomas in adults. Neuro-Oncol. 19(8):1127-1134. doi: 10.1093/neuonc/now274.

15- Louis DN, et al. (2018) CIMPACT-NOW Update 2: Diagnostic Clarifications for Diffuse Midline Glioma, H3 K27M-Mutant and Diffuse Astrocytoma/Anaplastic Astrocytoma, IDH-Mutant. *Acta Neuropathologica* 135(4): 639–42. doi: 10.1007/s00401-018-1826-y

16- Wesseling P and Capper D (2018) WHO 2016 Classification of Gliomas. Neuropathology and Applied Neurobiology 44(2): 139–50. doi: 10.1111/nan.12432

17- Aihara K, et al. (2014) H3F3A K27M mutations in thalamic gliomas from young adult patients. Neuro-Oncol 16:140–146. doi: 10.1093/neuonc/not144

18- Feng J, et al. (2015) The H3.3 K27M mutation results in a poorer prognosis in brainstem gliomas than thalamic gliomas in adults. Hum Pathol 46:1626–1632. doi: 10.1016/j.humpath.2015.07.002

19- Nakata S, et al. (2017) Histone H3 K27M mutations in adult cerebellar high-grade gliomas. Brain Tumour Pathol. 34(3):113-119. doi: 10.1007/s10014-017-0288-6.

20- Reyes-Botero G, et al. (2014) Molecular analysis of diffuse intrinsic brainstem gliomas in adults. J Neurooncol 116:405–411. doi: 10.1007/s11060-013-1312-2

21- Zhang L, et al. (2014) Exome sequencing identifies somatic gain-of-function PPM1D mutations in brainstem gliomas. Nat Genet 46:726–730. doi: 10.1038/ng.2995

22- Ryall S, et al. (2016) Targeted detection of genetic alterations reveal the prognostic impact of H3K27M and MAPK pathway aberrations in paediatric thalamic glioma. Acta Neuropathol Commun 4:93. doi: 10.1186/s40478-016-0353-0

23- Mondesir J, et al. (2016) IDH1 and IDH2 mutations as novel therapeutic targets: current perspectives. J Blood Med 7:171–180. doi: 10.2147/JBM.S70716

24- Touat M, et al. (2015) Targeting FGFR Signaling in Cancer. Clin Cancer Res Off J Am Assoc Cancer Res 21:2684–2694. doi: 10.1158/1078-0432.CCR-14-2329

25- Theeler BJ, et al. (2015) Adult brainstem gliomas: Correlation of clinical and molecular features. J Neurol Sci 353:92–97. doi: 10.1016/j.jns.2015.04.014

26- Buczkowicz P, et al. (2014). Genomic analysis of diffuse intrinsic pontine gliomas identifies three molecular subgroups and recurrent activating ACVR1 mutations. Nat Genet. 46(5):451-6. doi: 10.1038/ng.2936

27- Taylor KR, et al. (2014). Recurrent activating ACVR1 mutations in diffuse intrinsic pontine glioma. Nat Genet. 46(5):457-61. doi: 10.1038/ng.2925

28- Wu G, et al.; St. Jude Children's Research Hospital-Washington University Pediatric Cancer Genome Project (2014). The genomic landscape of diffuse intrinsic pontine glioma and pediatric non-brainstem high-grade glioma. Nat Genet. 46(5)444-50. doi: 10.1038/ng.2938

29- Fontebasso AM, et al. (2014). Recurrent somatic mutations in ACVR1 in pediatric midline high-grade astrocytoma. Nat Genet. 46(5):462-6. doi: 10.1038/ng.2950

30- Bourgeois M, et al. (1999). Surgery of epilepsy associated with focal lesions in childhood. J Neurosurg. 90(5):833-42. doi: 10.3171/jns.1999.90.5.0833

31- Posti JP et al. (2015) Presenting Symptoms of Glioma in Adults. Acta Neurological Scandinavica 131(2):88-93. doi: 10.1111/ane.12285.

32- Greenberg MS. (2016) Handbook of Neurosurgery 8th Edition. Thieme Publisher

33- Young RM, et al. (2015) Current Trends in the Surgical Management and Treatment of Adult Glioblastoma. Ann Transl Med 3(9): 121. doi: 10.3978/j.issn.2305-5839.2015.05.10

34- Liu D et al. (2018) Entrectinib: An Orally Available, Selective Tyrosine Kinase Inhibitor for the Treatment of NTRK, ROS1, and ALK Fusion-Positive Solid Tumours. Therapeutics and Clinical Risk Management 14: 1247–52. doi: 10.2147/TCRM.S147381

35- Gatalica Z, Xiu J, Swensen J, and Vranic S. (2018) Molecular Characterization of Cancers with NTRK Gene Fusions. Modern Pathology 32(1): 147–53. doi: 10.1038/s41379-018-0118-3

36- Lasorella A, Sanson M and Iavarone A (2017) FGFR-TACC Gene Fusions in Human Glioma. Neuro-Oncology 19(4): 475–83. doi: 10.1093/neuonc/now240.

37- Di Stefano AL et al. (2015) Detection, Characterization, and Inhibition of FGFR-TACC Fusions in IDH Wild-Type Glioma. Clinical Cancer Research 21(14): 3307–17. doi: 10.1158/1078-0432.CCR-14-2199.

38- Associazione Italiana di Oncologia Medica. (2016) "Linee Guida Neoplasie Cerebrali Edizione 2016." Linee guida Neoplasie Cerebrali: 38–42.

39- Reinhardt A, Stichel D, Schrimpf D et al (2018) Anaplastic astrocytoma with piloid features, a novel molecular class of IDH wildtype glioma with recurrent MAPK pathway, CDKN2A/B and ATRX alterations. Acta Neuropathol 136:273-291. doi: 10.1007/s00401-018-1837-8

40- Alexandrov LB, Nik-Zainal S, Wedge DC et al (2013) Signatures of mutational processes in human cancer. Nature 500:415-21. doi: 10.1038/nature12477.

41- Ostrom QT, et al. (2014). CBTRUS statistical report: primary brain and central nervous system tumours diagnosed in the United States in 2007-2011. Neuro Oncol. 16 Suppl 4:iv1-63. doi: 10.1093/neuonc/nou223

42- Rodriguez FJ, et al. (2010) Anaplasia in pilocytic astrocytoma predicts aggressive behavior. Am J Surg Pathol. 34(2):147-60. doi: 10.1097/PAS.0b013e3181c75238.

43- Jones DT, et al. (2008). Tandem duplication producing a novel oncogenic BRAF fusion gene defines the majority of pilocytic astrocytomas. Cancer Res. 68(21):8673-7. doi: 10.1158/0008-5472.CAN-08-2097.

44- Jones DT, et al. International Cancer Genome Consortium PedBrain Tumour Project (2013). Recurrent somatic alterations of FGFR1 and NTRK2 in pilocytic astrocytoma. Nat Genet. 45(8):927-32. doi: 10.1038/ng.2682.

45- Singh D, et al. (2012). Transforming fusions of FGFR and TACC genes in human glioblastoma. Science. 337(6099)4231-5. doi: 10.1126/science.1220834.

46- Collins VP, Jones DT and Giannini C (2015). Pilocytic astrocytoma: pathology, molecular mechanisms and markers. Acta Neuropathol. 129(6):775-88. doi: 10.1007/s00401-015-1410-7.

47- Merchant TE, et al. (2009). Conformal radiotherapy after surgery for paediatric ependymoma: a prospective study. Lancet Oncol. 10:258–266. doi: 10.1016/S1470-2045(08)70342-5

48- Figarella-Branger D, et al. (2000). Prognostic factors in intracranial ependymomas in children. J Neurosurg. 93(4):605-13. doi:10.3171/jns.2000.93.4.0605

49- Kilday JP, et al. (2009). Pediatric ependymoma: biological perspectives. Mol Cancer Res. 7(6)765-86. doi: 10.1158/1541-7786.MCR-08-0584.

50- Korshunov A, et al. (2010). Molecular staging of intracranial ependymoma in children and adults. J Clin Oncol. 28(19):3182-90. doi: 10.1200/JCO.2009.27.3359

51- Mack SC, et al. (2014). Epigenomic alterations define lethal CIMP-positive ependymomas of infancy. Nature. 506(7489):445-50. doi: 10.1038/nature13108.

52- Pajtler KW, et al. (2015). Molecular Classification of Ependymal Tumours across All CNS Compartments, Histopathological Grades, and Age Groups. Cancer Cell. 27(5):728-43. doi: 10.1016/j.ccell.2015.04.002.

53- Blümcke I and Wiestler OD (2002). Gangliogliomas: an intriguing tumour entity associated with focal epilepsies. J Neuropathol Exp Neurol. 61 (7):575-84. doi: 10.1093/jnen/61.7.575

54- Luyken C, et al. (2004). Supratentorial gangliogliomas: histopathologic grading and tumour recurrence in 184 patients with a median follow-up of 8 years. Cancer. 101(1):146-55. doi: 10.1002/cncr.20332.

55- Schindler G, et al. (2011). Analysis of BRAF V600E mutation in 1,320 nervous system tumours reveals high mutation frequencies in pleomorphic xanthoastrocytoma, ganglioglioma and extra-cerebellar pilocytic astrocytoma. Acta Neuropathol. 121 (3):397-405. doi: 10.1007/s00401-011-0802-6.

56- Chappe C, al. (2013). Dysembryoplastic neuroepithelial tumours share with pleomorphic xanthoastrocytomas and gangliogliomas BRAF(V600E) mutation and expression. Brain Pathol. 23(5):574-83. doi: 10.1111/bpa.12048.

57- Koelsche C, et al. (2013). Mutant BRAF V600E protein in ganglio- glioma is predominantly expressed by neuronal tumour cells. Acta Neuropathol. 125(6):891-900. doi: 10.1007/s00401-013-1100-2.

58- Padovani L, et al. (2012). Search for distinctiv e markers in DNT and cortical grade II glioma in children: same clinicopathological and molecular entities? Curr Top Med Chem. 12(15):1683-92. doi: 10.2174/156802612803531450.

59- Prabowo AS, et al. (2015). Landscape of chromosomal copy number aberrations in gangliogliomas and dysembryoplastic neuroepithelial tumours. Neuropathol Appl Neu- robiol. 41 (6):743-55. doi: 10.1111/nan.12235.

60- Prabowo AS, et al. (2014). BRAF V600E mutation is associated with mTOR signaling activation in glioneuronal tumours. Brain Pathol. 24(1):52-66. doi: 10.1111/bpa.12081.

61- Cocco E, Scaltriti M and Drilon A (2018) NTRK Fusion-Positive Cancers and TRK Inhibitor Therapy. Nature Reviews Clinical Oncology 15(12): 731–47. doi: 10.1038/s41571-018-0113-0.

62- Jones C and Baker SJ (2014) Unique Genetic and Epigenetic Mechanisms Driving Paediatric Diffuse High-Grade Glioma. Nature Reviews Cancer 14(10): 651–61. doi: 10.1038/nrc3811

63- Amatu A, Sartore-Bianchi A and Siena S (2016). NTRK Gene Fusions as Novel Targets of Cancer Therapy across Multiple Tumour Types. ESMO open 1(2): e000023. doi: 10.1136/esmoopen-2015-000023

64- Jimenez-Pascual A and Siebzehnrubl FA. (2019) Fibroblast Growth Factor Receptor Functions in Glioblastoma. Cells 13;8(7). pii: E715. doi: 10.3390/cells8070715.

65- Haugsten EM, et al. (2010) Roles of fibroblast growth factor receptors in carcinogenesis. Mol. Cancer Res. 8(11):1439-52. doi: 10.1158/1541-7786.MCR-10-0168.

66- Greulich H and Pollock PM. (2011) Targeting mutant fibroblast growth factor receptors in cancer. Trends Mol. Med. 17(5):283-92. doi: 10.1016/j.molmed.2011.01.012.

67- Costa R, et al. (2016) FGFR3-TACC3 fusion in solid tumours: Mini review. Oncotarget 7(34):55924-55938. doi: 10.18632/oncotarget.10482.

68- Lasorella A, Sanson M and Iavarone A. (2017) FGFR-TACC gene fusions in human glioma. Neuro Oncol. 19(4):475-483. doi: 10.1093/neuonc/now240.

69- Dienstmann R, et al. (2014) Genomic aberrations in the FGFR pathway: Opportunities for targeted therapies in solid tumours. Ann. Oncol. 25(3):552-63. doi: 10.1093/annonc/mdt419.

70- Singh D, et al. (2012) Transforming fusions of FGFR and TACC genes in human glioblastoma. Science. 337(6099):1231-5. doi: 10.1126/science.1220834.

71- Fukai J, et al. (2008) EphA4 promotes cell proliferation and migration through a novel EphA4-FGFR1 signaling pathway in the human glioma U251 cell line. Mol. Cancer Ther. 7(9):2768-78. doi: 10.1158/1535-7163.MCT-07-2263.

72- Loilome W, et al. (2009) Glioblastoma cell growth is suppressed by disruption of fibroblast growth factor pathway signaling. J. Neuro Oncol. 94(3):359-66. doi: 10.1007/s11060-009-9885-5.

73- Gouaze-Andersson V, et al. (2016) FGFR1 induces glioblastoma radioresistance through the PLCgamma/Hif1alpha pathway. Cancer Res. 76(10):3036-44. doi: 10.1158/0008-5472.CAN-15-2058.

74- Hale JS, et al. (2019) ADAMDEC1 maintains a novel growth factor signaling loop in cancer stem cells. Cancer Discov. 9(11):1574-1589. doi: 10.1158/2159-8290.CD-18-1308.

75- Picca A, et al. FGFR1 actionable mutations, molecular specificities, and outcome of adult midline gliomas. Neurology 2018; 90:e2086-e2094. doi:10.1212/WNL.0000000000005658

76- Trisolini E, et al. (2019) Actionable FGFR1 and BRAF mutations in adult circumscribed gliomas. J Neurooncol. 145(2):241-245. doi: 10.1007/s11060-019-03306-9.

77- Ostrom QT, et al. (2015) CBTRUS Statistical Report: Primary Brain and Central Nervous System Tumours Diagnosed in the United States in 2008-2012. Neuro-Oncology 17 Suppl 4:iv1-iv62. doi: 10.1093/neuonc/nov189.

78- Kleinschmidt-DeMasters BK and Mulcahy Levy JM (2018) H3 K27M-mutant gliomas in adults vs. children share similar histological features and adverse prognosis. Clinical Neuropathology 37(2):53-63. doi: 10.5414/NP301085.

79- Meel MH, Kaspers GJL and Hulleman E (2019) Preclinical therapeutic targets in diffuse midline glioma. Drug Resistance Updates 44:15-25. doi: 10.1016/j.drup.2019.06.001.

80- Stupp R et al. (2005) Radiotherapy plus Concomitant and Adjuvant Temozolomide for Glioblastoma. N Engl J Med 352(10): 987–96. doi: 10.1056/NEJMoa043330

81- Gessi M, et al. (2015) High frequency of H3F3A K27M mutations characterizes pediatric and adult high-grade gliomas of the spinal cord. Acta Neuropathol (Berl) 130:435–437. doi: 10.1007/s00401-015-1463-7

82- Salmaggi A, et al. (2008) Natural history and management of brainstem gliomas in adults. A retrospective Italian study. J Neurol 255:171–177. doi: 10.1007/s00415-008-0589-0

83- Mellinghoff IK, et al. (2016) ACTR-46. AG120, a first-in-class mutant idh1 inhibitor in patients with recurrent or progressive idh1 mutant glioma: results from the phase 1 glioma expansion cohorts. Neuro-Oncol 18:vi12-vi12. doi: 10.1093/neuonc/now212.044

84- Rohle D, et al. (2013) An inhibitor of mutant IDH1 delays growth and promotes differentiation of glioma cells. Science 340:626–630. doi: 10.1126/science.1236062

85- Babina IS and Turner NC (2017) Advances and challenges in targeting FGFR signalling in cancer. Nat Rev Cancer 17:318–332. doi: 10.1038/nrc.2017.8

86- Gessi M, et al. (2014) FGFR1 mutations in Rosette-forming glioneuronal tumours of the fourth ventricle. J Neuropathol Exp Neurol 73:580–584. doi: 10.1097/NEN.0000000000000080

87- Lin FY, et al. (2016) Integrated tumour and germline whole-exome sequencing identifies mutations in MAPK and PI3K pathway genes in an adolescent with rosette-forming glioneuronal tumour of the fourth ventricle. Cold Spring Harb Mol Case Stud 2:a001057. doi: 10.1101/mcs.a001057

88- Rivera B, et al. (2016) Germline and somatic FGFR1 abnormalities in dysembryoplastic neuroepithelial tumours. Acta Neuropathol (Berl) 131:847–863. doi: 10.1007/s00401-016-1549-x

89- Becker AP, et al. (2015) KIAA1549: BRAF Gene Fusion and FGFR1 Hotspot Mutations Are Prognostic Factors in Pilocytic Astrocytomas. J Neuropathol Exp Neurol 74:743–754. doi: 10.1097/NEN.0000000000000213

90- Brokinkel B, et al. (2015) A comparative analysis of MAPK pathway hallmark alterations in pilocytic astrocytomas: age-related and mutually exclusive. [corrected]. Neuropathol Appl Neurobiol 41:258–261. doi: 10.1111/nan.12145

91- Dyson K, et al. (2016) FGFR1 N546K and H3F3A K27M mutations in a diffuse leptomeningeal tumour with glial and neuronal markers. Histopathology 69:704–707. doi: 10.1111/his.12983

92- Schwartzentruber J, et al. (2012) Driver mutations in histone H3.3 and chromatin remodelling genes in paediatric glioblastoma. Nature 482:226–231. doi: 10.1038/nature10833

93- Rand V, et al. (2005) Sequence survey of receptor tyrosine kinases reveals mutations in glioblastomas. Proc Natl Acad Sci U S A 102:14344–14349. doi: 10.1073/pnas.0507200102

94- Lew ED, et al. (2009) The precise sequence of FGF receptor autophosphorylation is kinetically driven and is disrupted by oncogenic mutations. Sci Signal 2:ra6. doi: 10.1126/scisignal.2000021

95- Bennett JT, et al. (2016) Mosaic Activating Mutations in FGFR1 Cause Encephalocraniocutaneous Lipomatosis. Am J Hum Genet 98:579–587. doi: 10.1016/j.ajhg.2016.02.006

96- A Dose Finding Study Followed by a Safety and Efficacy Study in Patients With Advanced Solid Tumours or Multiple Myeloma With FGF/FGFR-Related Abnormalities - Full Text View - ClinicalTrials.gov. https://clinicaltrials.gov/ct2/show/NCT02052778. Accessed 4 Aug 2017

97- Ochiiwa H, et al. (2013) Abstract A270: TAS-120, a highly potent and selective irreversible FGFR inhibitor, is effective in tumours harboring various FGFR gene abnormalities. Mol Cancer Ther 12:A270–A270. doi: 10.1158/1535-7163.TARG-13-A270

98- Joyon N, et al. (2017) K27M mutation in H3F3A in ganglioglioma grade I with spontaneous malignant transformation extends the histopathological spectrum of the histone H3 oncogenic pathway. Neuropathol Appl Neurobiol 43:271–276. doi: 10.1111/nan.12329

99- Nguyen AT, et al. (2015) Evidence for BRAF V600E and H3F3A K27M double mutations in paediatric glial and glioneuronal tumours. Neuropathol Appl Neurobiol 41:403–408. doi: 10.1111/nan.12196

100- Pagès M, et al. (2016) Co-occurrence of histone H3 K27M and BRAF V600E mutations in paediatric midline grade I ganglioglioma. Brain Pathol Zurich Switz. doi: 10.1111/bpa.12473

101- Vaishnavi A, Le AT and Doebele RC. (2015) TRKing down an Old Oncogene in a New Era of Targeted Therapy. Cancer Discovery 5(1):25-34. doi: 10.1158/2159-8290.CD-14-0765.

102- Cook PJ, et al. (2017) Somatic chromosomal engineering identifies BCAN-NTRK1 as a potent glioma driver and therapeutic target. Nat Commun. 8:15987. doi: 10.1038/ncomms15987.

103- Xu T, et al. (2018) Gene Fusion in Malignant Glioma: An Emerging Target for Next-Generation Personalized Treatment. Translational Oncology 11(3):609-618. doi: 10.1016/j.tranon.2018.02.020.

104- Jones DT, et al. (2012) MAPK pathway activation in pilocytic astrocytoma. Cell Mol Life Sci 69:1799–1811. doi: 10.1007/s00018-011-0898-9.

105- Pathak P, et al. (2017) Genetic alterations related to BRAF-FGFR genes and dysregulated MAPK/ERK/mTOR signaling in adult pilocytic astrocytoma. Brain Pathol 27:580–589. doi: 10.1111/bpa.12444.

106- Smith KM, et al. (2006) Midline radial glia translocation and corpus callosum formation require FGF signaling. Nat Neurosci 9:787–797. doi: 10.1038/nn1705

107- Hébert JM, Lin M, Partanen J, Rossant J, McConnell SK (2003) FGF signaling through FGFR1 is required for olfactory bulb morphogenesis. Development 130:1101–1111. doi: 10.1242/dev.00334

108- Jones DT, et al. (2009) Oncogenic RAF1 rearrangement and a novel BRAF mutation as alternatives to KIAA1549:BRAF fusion in activating the MAPK pathway in pilocytic astrocytoma. Oncogene 28:2119–2123. doi: 10.1038/onc.2009.73.

109- Eisenhardt AE, et al (2011) Functional characterization of a BRAF insertion mutant associated with pilocytic astrocytoma. Int J Cancer 129:2297–2303. doi: 10.1002/ijc.25893.

110- Hou P, Liu D and Xing M (2007) Functional characterization of the T1799–1801del and G1799–1816ins BRAF mutations in papillary thyroid cancer. Cell Cycle 6:377–379. doi: 10.4161/cc.6.3.3818